Josua Bächle, BSc

An ESR and ENDOR investigation on the radical cation of zinc-5,10,15,20-tetraphenyl-21H,23H-porphyrine

MASTERARBEIT

zur Erlangung des akademischen Grades

Master of Science

Masterstudium Chemie

eingereicht an der

Technischen Universität Graz

Betreuer

O.Univ.-Prof. Dipl.-Ing. Dr.rer.nat. Günter Grampp

Physikalische und Theoretische Chemie

optionales Feld (Zweitbetreuer/in, Fakultätsnr., etc) max. 2-zeilig

Graz, Mai 2014

EIDESSTATTLICHE ERKLÄRUNG

AFFIDAVIT

Ich erkläre an Eides statt, dass ich die vorliegende Arbeit selbstständig verfasst, andere als die angegebenen Quellen/Hilfsmittel nicht benutzt, und die den benutzten Quellen wörtlich und inhaltlich entnommenen Stellen als solche kenntlich gemacht habe. Das in TUGRAZonline hochgeladene Textdokument ist mit der vorliegenden Masterarbeit identisch.

I declare that I have authored this thesis independently, that I have not used other than the declared sources/resources, and that I have explicitly indicated all material which has been quoted either literally or by content from the sources used. The text document uploaded to TUGRAZonline is identical to the present master‘s thesis.

Datum / Date

Unterschrift / Signature

I would like to thank

Günter Grampp, my supervisor, who did not just permit this work, but always had time for inspiring discussions, useful advice and practical demonstrations. Further I want to thank him for showing me more of the world than I knew.

Kenneth, my friend and mentor, who always found time to discuss work, God and the world and never hesitated to ask inconvenient questions.

Boryana, who taught me how to operate the different experimental setups, and Beate for patiently sharing the Bruker machine with me.

Hilde, who helped me in the lab, reminded me of working carefully and patiently explained where to find things.

Marion for all the help with the administrational necessities.

My colleagues and friends at the TU Graz who I have the pleasure to know.

My family for always believing in me.

Preface

Metal porphyrins play a vital role in biological electron transfer systems. The active site of chlorophyll e.g. is a Manganese-(II)-complex of this kind. Therefore these substances have become of great interest in electrochemical research. However, hardly any ESR data concerning electron self-exchange rates, which are useful parameters for prediction of electron transfer rate constants in Marcus theory, is available. On one hand this is related to their very complex hyperfine structure, on the other to various problems with the chemical generation of the radical. [1]

Further these substances have interesting photochemical properties, which are currently investigated by the international EU-FWF-VERANET-Program. In the framework of this program our group has a cooperation with the group of Professor Otto Horvarth in Veszprém (Hungary), who synthesizes new metal porphyrin complexes. Therefore a method to investigate these compounds properly by ESR spectroscopy is desired.

In 2003 S. Fukuzumi et al published electron self-exchange rates [2, 3] of two substituted zinc porphyrins with their corresponding radical cations. They reported those to be extremely fast due to very small activation energies, which he found to be close to zero. For some of the investigated systems it was even negative. This behavior is rarely observed in chemistry and for electron self-exchange it has been reported only for a few systems so far. [4] Therefore it appeared to be a reasonable starting point for testing our methods. Unfortunately the results of Fukuzumi et al are not reproducible. The aim of this thesis is a critical theoretical and experimental evaluation of Fukuzumi´s group results, where the zinc-5,10,15,20-tetraphenyl-21H,23H-porphyrine (ZnTPP) was chosen develop a method for ESR investigations on metal porphyrins in general.

The thesis is arranged in four parts, where the first three cover the relevant theoretical aspects needed to understand the investigated process and the utilized experimental methods. The basic electron transfer theory was acquired mainly from the Nobel lecture of R. A. Marcus [5] and a review article by N. Sutin. [6] Further publications, which contain more detailed information, are cited explicitly. The theory of ESR spectroscopy was acquired from two textbooks [7, 8]. The theory of ENDOR spectroscopy was taken from a special textbook on this method. [9] Every illustration taken from these books is labeled explicitly, the others are self-drawn.

In experimental part results for different approaches to generate the radical and ENDOR measurements are presented and discussed in respect to previous results, with a critical view on the work of Fukuzumi, which turned out as being irreproducible. Finally a reproducible method is introduced as basis for further line broadening experiments.

Contents

Part 1: Theory of Electron Transfer

1.1 Introduction

Even though electron transfer (ET) appears to be quite simple, it plays a major role in nature and technology. Many vitally important processes such as photosynthesis or the respiratory chain include long reaction chains of consecutive ETs. Every electrochemical power supply performs countless numbers of ETs during their operation time and a large number of other examples of the application of ETs could be given. Therefore the quest for a comprehensive understanding has become the goal of many theorists and experimentalists in different fields of science during the last decades.

To study chemical processes from a mechanistic point of view usually kinetic data is measured, which helps to narrow down possibilities. Unfortunately most ETs are very fast compared to other chemical processes because bond breaking or formation is in most cases not necessary. Therefore ETs where simply too fast for the instrumentation available before World War II.

When the post-war instrumentation became accessible in chemical laboratories methods were developed and improved. Especially in respect to time resolution great progress was achieved during the late 1940s and 1950s. As a result of that first experimental data on kinetics of ETs were published by N. Sutin or B. Libby e.g. to name a few important pioneers in this field.

The discussion of their results inspired R.A. Marcus to formulate his still valid theory on ET, which will be referred to as Marcus Theory, in 1956, for which he received the Nobel Prize in chemistry in 1992. The further development of his initial theory and the experimental validation of its predictions is a still ongoing process.

In the following the basic aspects of Marcus Theory and its most important implementations will be discussed, with a special focus on electron self-exchange reactions in solution, since this type of reaction was investigated in the experimental section.

1.2 Basic Assumptions of Marcus Theory

In his Nobel lecture [5] Marcus gives a nice summary of the circumstances that led to the formulation of his theory, which was published in 1956 [10] and readily expanded. [11, 12] This theory is still applied to describe experimental results of various ET processes.

He especially highlights a previous publication of W.F. Libby on the electron self-exchange of metal complexes. [13] This was the first time that the idea of introducing the Franck-Condon in the description of a chemical reaction was formulated.

To illustrate this the picture of a charged molecule in a polar solvent is used. It is known, that the positions of the atoms relative to each other differ with the oxidation state of the molecule, as well as the orientation of the solvent dipoles around it. If the electron would just jump, a process much faster than the reorientation of all atoms and solvent molecules, it would be in a surrounding where it is not stabilized. Therefore a very large amount of energy would have to be added from the outside to satisfy the first law of thermodynamics. The only way to do this is by absorption of light, meaning ET cannot happen in the dark, which is not in agreement to experiments.

Marcus generally assumed the ET to be an activated process following a three step pathway given in figure 1.

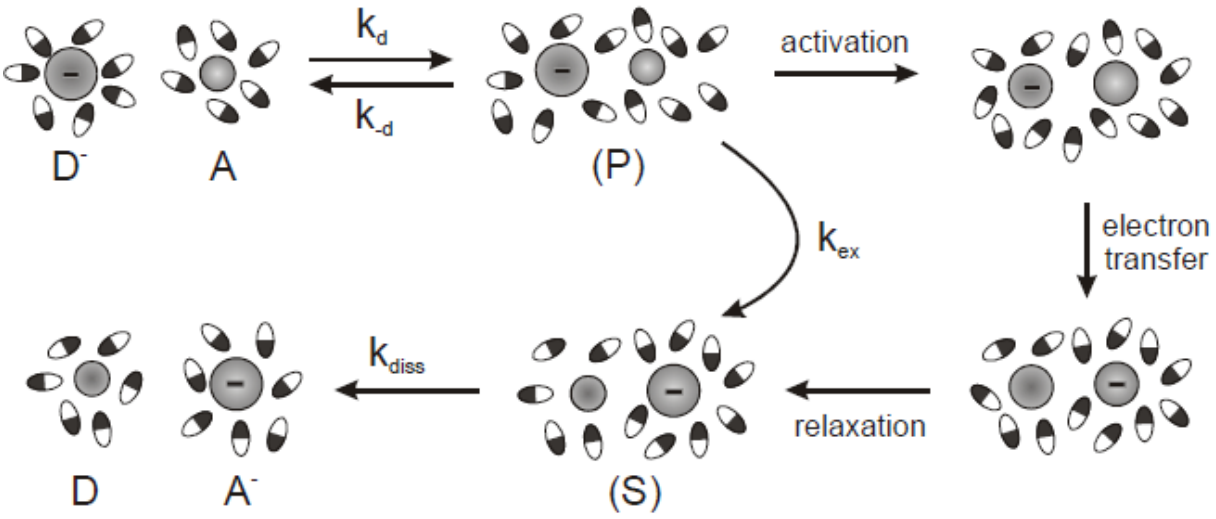

Figure 1: General reaction mechanism of ET

The first step is the diffusion of a Donor D and an Acceptor A towards each other, where the drawn *charge* just marks the position of the electron being transferred. At a certain distance a small orbital overlap between A and D can occur, thus the so called precursor complex P is formed. The surrounding solvent dipoles around P are not corresponding to the equilibrium orientation of A and D alone anymore; the same applies for the orientation of the atoms. From this initial state the actual transfer of the electron takes place, which is generally split in three parts, which are described by one kinetic constant k_{ET} nonetheless. First P has to be activated, which is related to a certain reorganization of the position of atoms due to small random

motions. When this point is reached the actual ET happens in an isoenergetic way at fixed positions and momenta of the atoms, satisfying the Franck-Condon Principle. Finally relaxation leads to the successor complex S, which dissociates in a third and final step, giving the products.

First of all step one and two of the proposed mechanism will be discussed further for a general ET between two different reactants. For exergonic reactions it is assumed that in the ET-step no back reaction happens. Furthermore the dissociation of S is mostly considered to be negligible fast.

1.3 The Association Reaction

The precursor complex is, as already mentioned, formed in a very simple picture by the collision of two reactants, which is reversible. This leads to an equilibrium between associated and free reactants in the solution. This can be expressed in terms of chemical kinetics according to equation (1.0), where K_A denotes the equilibrium constant.

$$K_A = \frac{k_d}{k_{-d}} \tag{1.0}$$

If one imagines the reactants to be uncharged spheres it is quite obvious, that in a given volume for a given number of bodies only their size is determining for the collision rate or the time they spend associated respectively, simply because the amount of free space is decreasing. Therefore a very simple association constant $K_{A,0}$ can be formulated in terms of a molar volume, as in equation (1.1). Here σ is the intermolecular distance associated with the free volume of the reactant, which also includes interactions with the solvent.

$$K_{A,0} = \frac{4\pi}{3} N_A \sigma^3 \tag{1.1}$$

This can be further improved to equation (1.2) by introducing a variable reaction sphere ∂σ, which is usually taken to be 80 pm. [14].

$$K_{A,0} = \frac{4\pi}{3} N_A \sigma^2 \partial\sigma \tag{1.2}$$

If both reactants have an electrical charge an additional electrostatic work term W must be included, which is known to be indirectly proportional to the intermolecular distance of the reactants and the solvent´s dielectric constant from Coulomb´s law. This was introduced by

M. Eigen and R. M. Fuoss independently from each other in the 1950s, as given in equation (1.3). [15, 16]

$$K_A = K_{A,0} * e^{-\frac{W}{RT}} \quad (1.3)$$

This rather simple picture can be refined by applying other models with more sophisticated approaches to describe the geometry of the reactants. Due to the low relevance of K_A to the experimental section this shall not be elaborated further in this thesis.

1.4 The Electron Transfer

In the theory of activated processes kinetic constants k are related to the so called activation energy ΔG*, also known as activation barrier, according to the general Arrhenius equation (1.4). [17] Here A denotes the so-called preexponential factor, which is discussed in respect to ET in chapter 1.9, k_B is the Boltzmann constant and T the absolute temperature.

$$k = A * e^{-\frac{\Delta G^*}{k_B T}} \quad (1.4)$$

Thus a theoretical expression of ΔG* is desirable to calculate chemical rate constants. ΔG* is generally defined as the difference of the total energy of the transition state (the precursor complex and his surrounding in a geometrical conformation related to a successor complex) and the energy of the reactants. For this discussion the precursor complex will be assumed to be the educt. Moreover the necessary energy of activation is considered to be relatively low, such that the transition state can be reached via small random nuclear motions.

To obtain the total energy of these states a wave function Ψ describing the reacting complex as a function of the positions of all atoms has to be constructed. In the case of a small orbital overlap this can be done by linear combination of two wave functions Ψ_1 and Ψ_2 (1.5). The former describes the two reactants, the latter two products, each far apart from each other in the solvent. The coefficient c is taken to be 1 in the transition state, since both configurations are assumed to contribute equally.

$$\varphi = \varphi_1 + c * \varphi_2 \quad (1.5)$$

Solving the Schrödinger equation for all possible atomic configurations gives a so called potential energy surface (PES) in 3N dimensions, where N denotes the number of atoms. The minima and maxima of the PES correspond to intermediates and transition states respectively.

Additionally the electrostatic interaction with the solvent has to be included. This is expressed in terms of the orientation of dipole moments, which is only ordered if a reactants or products is charged, due to their resulting electric field. For a single reactant in solution this is usually an equilibrium orientation. It is quite obvious that even though P and S have the same atomic configuration when the electron jumps, they differ tremendously in the distribution of electric charge. Considering the Born-Oppenheimer approximation no average equilibrium orientation of dipole moments in the transition state can exist. Therefore the in chapter 1.2 mentioned requirement of conservation of energy is only satisfied if one considers the total energy to be composed of the contributions from atomic configuration of the complex and from the orientation of solvent dipoles.

Considering this one can use quantum mechanical calculations, combined with time dependent perturbation theory to find the most likely intermediate with its corresponding transition state, marking the reaction pathway. In the approach of Marcus the solvent was treated as a polarizable electrostatic continuum and chemical bonds were approximated by harmonic oscillators.

A generic result of such calculations is displayed as a two-dimensional projection from the PES along this pathway in figure 2. Here ΔG^0 denotes the driving force of the reaction, V_{RP} is the so-called resonance splitting and λ is the so called reorganization parameter.

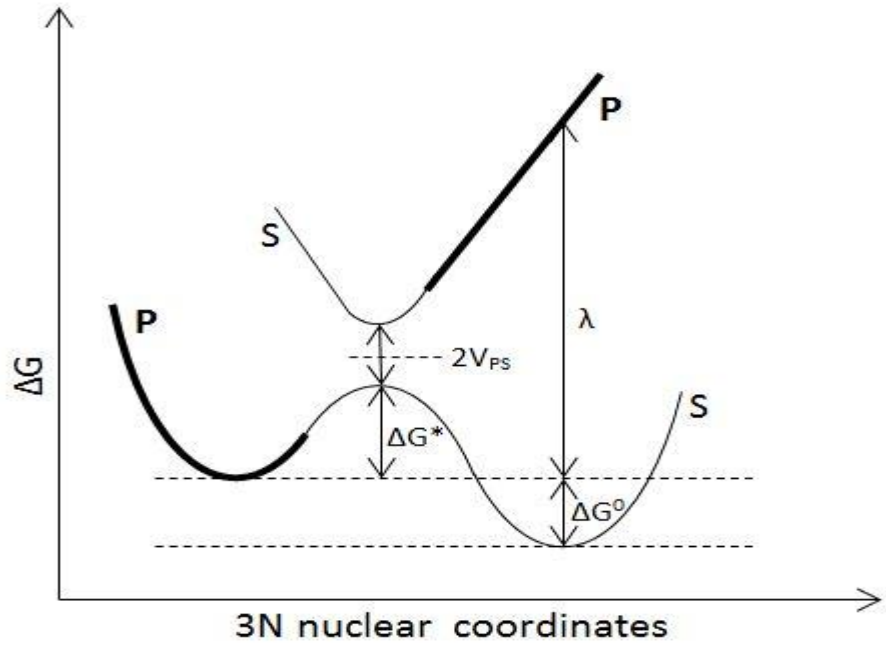

Figure 2: Two dimensional projection of ET on the PES

From the description of ET given in this chapter it is quite obvious, that the reorganization parameter λ is defined as the sum of two terms, one describing the reorganization of the atoms λ_i (Chapter 1.5) and one describing the reorientation of solvent dipoles λ_o. (Chapter 1.6)

Equation (1.6) gives Marcus´s famous expression for the activation energy ΔG* for an ET starting at P to form S in its simplest form. However, the resonance splitting and electron tunneling are neglected here.

$$\Delta G^* = \frac{\lambda}{4} * \left(1 + \frac{\Delta G^0}{\lambda}\right)^2 \qquad (1.6)$$

t is more convenient to express this in terms of the reactants, because there is hardly information on P or S available. Therefore the driving force for the overall reaction can be obtained from the difference redox potentials of the reactants E_A and E_D corrected as given in equation (1.7). F denotes Faradays constant, z_A and z_D the charge of the reactants, e_0 the elementary charge, f_{DH} the activity coefficient from Debye-Hückel theory, ε_S the dielectric constant of the solvent and σ the reaction distance.

$$\Delta G^0 = -F * (E_A - E_D) + (z_A - z_D + 1) * \frac{e_0^2 * f_{DH}}{\varepsilon_S * \sigma} \qquad (1.7)$$

Furthermore a work term W considering electrostatic interactions between reactants, given by Coulombs law, and the resonance splitting, which can be calculated by various quantum chemical methods, has to included, resulting in equation (1.8).

$$\Delta G^* = W + \frac{\lambda}{4} * \left(1 + \frac{\Delta G^0}{\lambda}\right)^2 - V_{PS} \qquad (1.8)$$

For electron self-exchange the driving force equals zero, because the educts and products are equal. Therefore equation (1.8) can be reduced to equation (1.9).

$$\Delta G^* = W + \frac{\lambda}{4} - V_{PS} \qquad (1.9)$$

1.5 The Inner Sphere Reorganization Energy

As already mentioned the precursor complex has to rearrange to a geometry corresponding to the successor complex. Therefore changes in bond lengths and angles are required. For rather simple systems this can be expressed by equation (1.10), where f denotes the force constant of a bond i and Δq the actual change in the bond length.

$$\lambda_i = \sum_i \frac{f_A^i * f_D^i}{f_A^i + f_D^i} * (\Delta q_i)^2 \qquad (1.10)$$

However, the difficulty of determining all the right vibrations contributing to the reaction path of question increases with the size and structural complexity, thus limiting the applicability of this model in respect to complex organic molecules. A solution for this problem was proposed by Nelsen et al. [18], who used semi-empirical AM1 calculations to calculate the energy of the reactants, transition state and products, which are related to λ_i as given in equation (1.11). Here E(A,D) means the energy of the acceptor in geometry of the donor and so on. One has to keep in mind that this method gives values of ΔH instead of ΔG, which is not considered to be a problem because the changes in entropy are hardly significant.

$$\lambda_i = [E(A,D) + E(D,A)] \; - \; [E(A,A) + E(D,D)] \qquad (1.11)$$

These approximations assume that the rearrangement of P to the geometry of S occurs completely. The probability of the system reaching this state is decreasing at lower temperature, thus increasing the possibility of tunneling through the activation barrier. This was introduced by Holstein [19] and further elaborated by several authors. An equation for λ_i including this aspect is given in literature. [6]

1.6 The Outer Sphere Reorganization Energy

The outer sphere reorganization energy describes the change in polarization of the solvent molecules in the surrounding of the activated complex. The total polarization consists of two parts. One is related to the electronic distribution in a molecule, which can be changed very fast by moving electron density along a bond e.g., what might lead to an induced dipole moment. The other one is associated with the orientation of permanent dipole moments. Changing this orientation requires the movement of the whole solvent molecule, which is very slow compared to the jump of an electron. Therefore this is the kinetically relevant part of the polarization. The general expression for this part, denoted as P_{slow}, is given in equation (1.12). Here ε_0 denotes the absolute dielectric constant, D the electric induction displacement and γ the so called Pekar factor, which is defined in equation (1.13). There ε_s denotes the static dielectric constant and n the refractive index.

$$\overrightarrow{P_{slow}} = \frac{\gamma}{4\pi\varepsilon_0} * \vec{D} \qquad (1.12)$$

$$\gamma = \frac{1}{n^2} - \frac{1}{\varepsilon_s} \tag{1.13}$$

Thus the energy associated with the change of P_{slow} is given by equation (1.14), which equals the outer sphere reorganization energy λ_o.

$$\lambda_o = \int [\overrightarrow{P_{slow}} d\vec{D}] dV \tag{1.14}$$

The solution of the integral in equation (1.14) for two spherical particles, where one is taken to be static, in close contact, meaning the reaction distance σ equals the sum of r_A and r_D, is given in equation (1.15).

$$\lambda_o = \frac{e_0^2 \gamma}{4\pi\varepsilon_0} * \left(\frac{1}{2r_A} + \frac{1}{2r_D} - \frac{1}{\sigma}\right) \tag{1.15}$$

1.7 Marcus Cross Relation

A very important aspect of Marcus Theory arises from the assumption that both reactants reorganize independently from each other. If this is true the overall reorganization energy for the whole reaction λ_{AD} is the sum of the reorganization energies of the two reactants, which can be obtained independently for each reactant from its self-exchange reaction by determining λ_{AA} and λ_{DD}. This is given in equation (1.16). The factor of ½ must be included due to the fact that in a self-exchange process the reorganization energy of two species (only differing in oxidation state) is determined, but only one of them contributes in a cross-reaction.

$$\lambda_{AD} = \frac{1}{2}\,(\lambda_{AA} + \lambda_{DD}) \tag{1.16}$$

The Marcus Cross Relation has been applied by several authors for various systems, showing a good correlation between theory and experiment. [20 – 22] This increases the importance of studying self-exchange reactions tremendously, especially because these reaction-systems are considerably simpler.

1.8 Marcus Inverted Region

Considering the fact that ΔG^0 of an exergonic reaction is per definition negative, equation (1.6) predicts a very unusual behavior for highly exergonic ET reactions, which is referred to as inverted region. A graphical summary of this effect is displayed in figure 3, where the resonance splitting has not been drawn.

As long as the requirement $\Delta G^0 > -\lambda$ is fulfilled, the activation barrier is lowered with increasing exergonic character of the reaction, thus the reaction rate is increasing. This is considered to be the normal region. The fastest reaction is happening when ΔG^0 equals λ because then no activation barrier is present. However, making the reaction more exergonic, where $\Delta G^0 < -\lambda$, suddenly slows the reaction down by increasing the activation barrier.

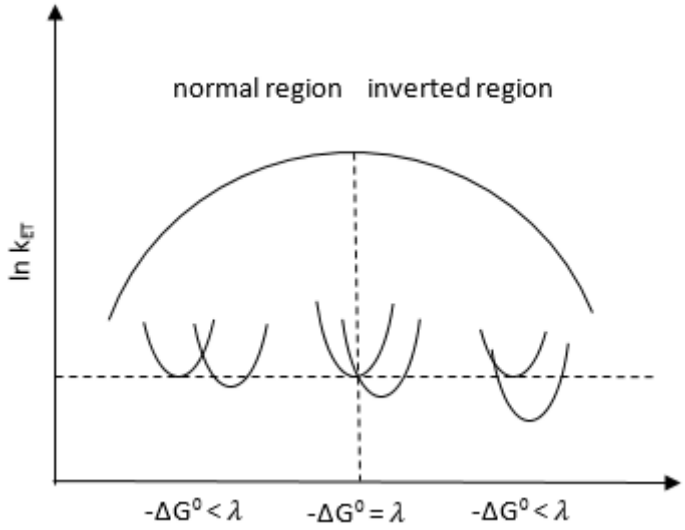

Figure 3: Graphical display of Marcus Inverted Region

Unfortunately most chemical systems are not exergonic enough to show an inverted region effect, therefore the experimental proof, first given by J.R. Miller, [23] was published 30 years later.

1.9 Kinetics of Electron Transfer and Electron Self Exchange

In equation (1.17) the process of a homogeneous ET between two different reactants is displayed in terms of chemical reaction equations. A general expression for the ET rate constant k_{ET} will be derived based on that.

$$A + D \underset{k_{-d}}{\overset{k_d}{\rightleftarrows}} P \underset{k_{-ex}}{\overset{k_{ex}}{\rightleftarrows}} S \xrightarrow{k_{diff}} products \qquad (1.17)$$

First of all an experiment to determine the rate of the overall rate constant k_{obs} is set up, where the formation of the products is monitored, thus equation (1.18) is valid.

$$k_{obs} * [A] * [D] = k_{diff} * [S] \qquad (1.18)$$

During the process the concentrations of P and S are considered to reach a steady state. The corresponding steady state conditions are formulated in equations (1.19) and (1.20).

$$\frac{\partial [P]}{\partial t} = 0 = k_d * [A] * [D] + k_{-ex} * [S] - (k_{ex} + k_{-d}) * [P] \qquad (1.19)$$

$$\frac{\partial[S]}{\partial t} = 0 = k_{ex} * [P] - \left(k_{-ex} + k_{diff}\right) * [S] \qquad (1.20)$$

Combining equation (1.18-1.20) as shown in Appendix A one obtains a general expression for k_{obs}, which is denoted in equation (1.21).

$$k_{obs} = k_d * \left[1 + \frac{k_{-d}}{k_{ex}} * \left(1 + \frac{k_{-ex}}{k_{diff}}\right)\right]^{-1} \qquad (1.21)$$

For a normal ET the back reaction is assumed to not occur, meaning k_{-ex} equals zero. Thus equation (1.21) simplifies to equation (1.22).

$$k_{obs} = \frac{k_d k_{ex}}{k_{-d} + k_{ex}} \qquad (1.22)$$

Furthermore k_{ET} is defined as given in equation (1.23), with KA given in equation (1.0). The dissociation of the successor complex is assumed to be negligibly fast in respect to the overall forward reaction.

$$k_{ET} = K_A * k_{ex} \qquad (1.23)$$

Substituting k_{ex} in equation (1.22) according to equation (1.23) one gains equation (1.24), which is the desired expression of k_{ET}. The usual interpretation of this equation is that experimental values of k_{obs} have to be corrected by diffusion. Unfortunately this correction is sometimes applied in literature [2] for electron self-exchange, where it is not valid because the requirement of k_{-ET} being equal to zero is not fulfilled.

$$\frac{1}{k_{ET}} = \frac{1}{k_{obs}} - \frac{1}{k_d} \qquad (1.24)$$

To describe the electron self-exchange one has to insert equation (1.23) directly in equation (1.21). Assuming that k_{ex} is equal to k_{-ex} and k_{-d} is equal to k_{diff}, which is reasonable due to the equivalence of educts and products, one ends up with the correct expression (1.25).

$$\frac{1}{k_{ET}} = \frac{1}{k_{obs}} - \frac{2}{k_d} \qquad (1.25)$$

The advantage of equations (1.24) and (1.25) is that k_{ET} is now only dependent on two variables, which can be measured. However, in the experimental section only k_{obs} will be determined experimentally. k_d will be obtained from the Smoluchowski equation (1.26), which describes diffusion in terms of Brownian motion. Here N_A denotes the Avogadro constant, D_i the diffusion coefficient and r_i the radius of A and D, which are considered to be spherical.

$$k_d = 4\pi N_A * (D_A + D_D) * (r_A + r_D) \quad (1.26)$$

The Diffusion coefficients can be calculated from the Stokes-Einstein equation (1.27), which is given for the so-called *stick conditions*, meaning A and D are significantly larger than the solvent molecules. In the opposite case, which is referred to as *slick conditions*, a factor of 4 instead the one of 6 is used. The new variable η denotes the viscosity of the solvent.

$$D_i = \frac{k_B T}{6\pi r_i \eta} \quad (1.27)$$

In the case of electron self-exchange one usually assumes that $r_A = r_D$. Therefore equation (1.26) simplifies to equation (1.28).

$$k_d = \frac{8RT}{3\eta} \quad (1.28)$$

1.10 Solvent Dependence of Electron Transfer Kinetics

In chapter 1.4 the general Arrhenius equation (1.4) was mentioned to point out the importance of activation barriers on chemical rate constants. Alternatively for ET this can be expressed in terms of a nuclear κ_n, electronic κ_{el} and frequency factor ν_n, as shown in equation (1.29). [24] The nuclear factor κ_n is defined like the exponential part of the Arrhenius equation, hence the preexponential factor A is the product of ν_n and κ_{el}.

$$k_{ET} = \nu_n * \kappa_{el} * \kappa_n \quad (1.29)$$

In chapter 1.6 the direct proportionality between λ_o and γ, which quantifies the electrostatic properties of the solvent, was shown. Consequently higher polarity of the solvent increases the activation barrier in the exponential part of the Arrhenius equation, thus lowering the rate of ET.

However, this is not the only influence the solvent has on the rate of ET. The further presented effect, which appears in the preexponential factor, is presented in terms of the frequency factor ν_n only, because κ_{el} is a function of ν_n.

At this point it seems important to point out, that κ_{el} is also dependent on the resonance splitting V_{PS}. Dependent on the magnitude of V_{PS} one can distinguish two different types of ET, called diabatic for small values of V_{PS} and adiabatic for large values of V_{PS}.

In a classical model ν_n can be interpreted as the frequency of crossing the activation barrier. Thus it is related to the vibrations that destroy the configuration of the activated complex,

which is expressed in equation (1.30), where ν_i denotes every frequency of the i^{th} nuclear mode that contributes to ΔG*.

$$\nu_n = \sqrt{\frac{\sum_i (\nu_i^2 * \Delta G_i^*)}{\Delta G^*}} \tag{1.30}$$

Due to the fact that the ν_i refer to the solvent modes as well as to the ones from the precursor complex, equation (1.30) can be written in more detailed picture shown in equation (1.31). The contributions of the solvent and the precursor complex have been separated.

$$\nu_n = \sqrt{\frac{\sum_i \left[\left(\nu_{i,Sol}^2 * \lambda_o \right) + \left(\nu_{i,P}^2 * \lambda_i \right) \right]}{\lambda}} \tag{1.31}$$

This indicates that every nuclear motion from the collective solvent might influence the rate of ET, even though the high frequency modes of vibrations, which are related to the fast polarization mentioned in chapter 1.6, dominate tremendously.

Since the solvent participates as a collective in the ET, this influence is referred to as solvent friction. A comprehensive discussion of its implications was published by M. J. Weaver [25], who describes and evaluates all effects in more detail, than the classical picture given below.

The first significant influence of solvent friction was reported by H.A. Kramers. [26] This can be described in terms of the longitudinal relaxation time τ_L of the solvent, which is defined in equation (1.32). The new variables τ_D, V_m and ε_∞ are the Debye relaxation, which can be calculated from equation (1.33), the molar volume of the solvent and its infinite frequency dielectric constant respectively.

$$\tau_L = \tau_D * \frac{\varepsilon_\infty}{\varepsilon_s} \tag{1.32}$$

$$\tau_D = \frac{3\, V_m \eta}{RT} \tag{1.33}$$

Introducing this quantity with the assumptions of an adiabatic ET, where κ_{el} is defined to be one, and $\lambda_i < \lambda_o$, the nuclear frequency factor can be expressed by equation (1.34).

$$\nu_n = \frac{1}{\tau_L} * \sqrt{\frac{\lambda_o}{4\pi RT}} \tag{1.34}$$

Therefore the rate of ET increases with a lower longitudinal relaxation time of the solvent, which is as a function of η exponentially dependent on temperature.

For completeness the preexponential factor is given for a diabatic ET as well in equation (1.35), because here the value of κ_{el} is different to one. The new variable ħ denotes the reduced Planck constant.

$$\nu_n \kappa_{el} = \frac{2\pi V^2}{\hbar N_A \sqrt{4\pi \lambda_o RT}} \tag{1.35}$$

Part 2: Electron Spin Resonance

2.1 Introduction

From a theoretical approach Electron Spin Resonance (ESR) or Electron Paramagnetic Resonance (EPR) spectroscopy is closely related to Nuclear Magnetic Resonance (NMR) spectroscopy, because both methods utilize the magnetic Zeeman Effect.

In 1896 P. Zeeman [27] reported a splitting of lines in electronic spectra in the presence of a magnetic field, which could be explained by the angular momentum of an electron known from quantum mechanics. Further similar experiments by O. Stern and W. Gerlach in 1922 [28] and G.E. Uhlenbeck and S. Goudsmith in 1925 [29], which could not be explained like Zeemans findings, led to the formulation of the spin as a fundamental concept in quantum mechanics.

The tremendous progress in radar technology during World War II enabled K. Zavoisky to record the first ESR spectrum ever reported in 1944. [30] Henceforward, the theoretical understanding and instrumental techniques developed rather fast over the following decades. In 1956 G. Feher reported the first successful double resonance experiment [31], which will be discussed in part 3 of this thesis. Further developments in the field of pulsed techniques or the discovery of the effect of chemically induced dynamic polarisation in experiments using lasers are mentioned for reasons of completeness.

All these methods enabled and still enable scientists to obtain structural and dynamic information of paramagnetic systems, which are necessary to understand chemical processes on a more fundamental level. Furthermore ESR spectroscopy found its applications in qualitative and quantitative analytics. For the former the limitation of this technique on paramagnetic systems is a great advantage in terms of sensitivity, which is guaranteed up to relatively low limits of detection. However, the latter has its drawbacks, due to the fact that here the intensity of absorption is dependent on many factors, which will be discussed later.

2.2 Fundamentals of Magnetic Resonance

Magnetic resonance is basically the absorption of electromagnetic radiation, which for ESR experiments happens to be in the energetic region of microwaves, due to the interaction of its magnetic component with certain magnetic moments in matter, which are oriented along an external magnetic field.

These magnetic moments $\vec{\mu}_e$, which can be calculated from equation (2.1) for a single electron, will be described in terms of the vector model. Here m_e and e_0 denote mass and charge of an electron, g_e is the so called g-factor and $\vec{S}$ is the quantum mechanical spin vector.

$$\vec{\mu}_e = -\frac{g_e * e_0}{2m_e} * \vec{S} \qquad (2.1)$$

In nuclear physics the magnetic moment of an electron is usually expressed in units of the Bohr magneton μ_B, which is defined in equation (2.2), where h denotes the Planck constant. Considering this one readily obtains equation (2.3).

$$\mu_B = -\frac{h * e_0}{4\pi * m_e} \approx 9{,}274 * 10^{-24}\, J/T \qquad (2.2)$$

$$\vec{\mu}_e = -\frac{2\pi * g_e * \mu_B}{h} * \vec{S} \qquad (2.3)$$

The only quantity determining the magnitude of the magnetic moment of an electron is the length of the spin vector $\vec{S}$ independent of the convention one uses to describe the magnetic moment of an electron. It can be expressed by equation (2.4), where S denotes the spin quantum number, which for an electron always has the value of 1/2.

$$\overrightarrow{|S|} = \frac{h}{2\pi}\sqrt{S\,(S+1)} \qquad (2.4)$$

In a classical or mathematical approach the spin can be understood in terms of an orbital angular momentum. In this picture the induction of a magnetic moment, due to the electric charge of an electron is quite obvious. It is known from the Pauli principle that electron spins in atoms and chemical bonds tend to be in a paired state, where their magnetic moments cancel each other. This explains the limitation of ESR to paramagnetic systems, which contain per definition at least one unpaired electron spin.

For magnetic resonance experiments an external magnetic field is required to generate energetically different spin states, which is called the Zeeman Effect. This field is usually depicted as a field of vectors pointing from the North to the South Pole of a magnet, which are present in the whole surrounding space. In a significantly small volume this magnetic field lines can be assumed to be approximately parallel directly in between the poles. Additionally their direction is fixed along the z-axis of a Cartesian coordinate system for further purposes. The density of these lines is referred to as the magnetic field strength $\vec{H}$. However, the actual magnetic field the magnetic moment of an electron experiences is given by the magnetic flux

density $\vec{B}$, which is defied in equation (2.5). There μ_m denotes the magnetic permeability, which is an intrinsic property of a material.

$$\vec{B} = \vec{H} * \mu_m \tag{2.5}$$

Figure 4 shows the possible orientations for an electrons magnetic moment, which is defined to point from South to North Pole, in an external magnetic field. The rotation around the field lines indicated in this picture is referred to as Larmor precession, defined in equation (2.34), which is of fundamental importance in the analysis of molecular structures by chemical shifts in NMR spectroscopy.

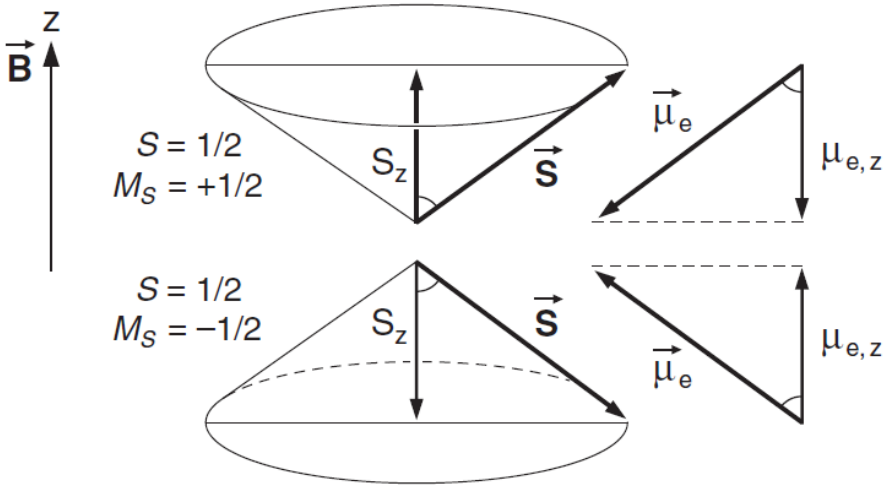

Figure 4: Orientation of an electrons magnetic moment in an external field [8]

The number of possible orientations is given by the multiplicity M, which is denoted in equation (2.6).

$$M = 2S + 1 \tag{2.6}$$

Furthermore new magnetic quantum numbers m_s are assigned to describe these orientations, following a general scheme {+S, S-1, ... -S}. These orientations will be called spin states for further purposes. Thus an electron with S = ½ has two possible spin states with $m_s = \pm ½$. The spin state with $m_s = +½$ is usually called *spin up* or α, the other *spin down* or β. The magnitude of z-components of $\vec{S}$ and $\vec{\mu_e}$ is defined in equation (2.7) and (2.8). The latter is obtained from equation (2.3) and (2.7).

$$S_z = \frac{h}{2\pi} * m_s \tag{2.7}$$

$$\mu_{e,z} = -\, g_e * \mu_B * \, m_s \tag{2.8}$$

Equation (2.7) can be used to calculate the angle θ as 54.73° between $\vec{B}$ and $\vec{S}$ by simple trigonometry.

From a classical physical point of view one can describe these new spin states as simple permanent magnets in a magnetic field shown in figure 5. The orientation dependent energy of those is given in equation (2.9).

$$E = -\vec{\mu} * \vec{B} \cos\theta \tag{2.9}$$

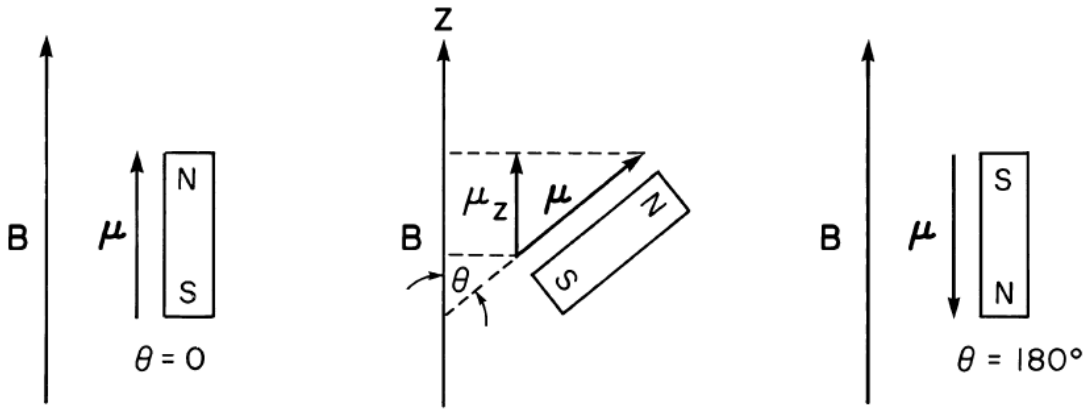

Figure 5: Orientation of a classic permanent magnet moment in an external field [7]

To get rid of the cosine in equation (2.9) the z-component of $\vec{\mu}_e$ from equation (2.8) is used to obtain a general expression for the energy E of the spin states, which is given in equation (2.10). Thus the difference in energy can be calculated from equation (2.11), where for an electron Δm_s is equal to one.

$$E = m_s * g_e * \mu_B * \vec{B} \tag{2.10}$$

$$\Delta E = \Delta m_s * g_e * \mu_B * \vec{B} \tag{2.11}$$

Absorption occurs when the energy of an electromagnetic wave given by the product of the Planck constant h and its frequency ν is equal to ΔE from equation (2.11). Thus the so-called resonance condition can be formulated according to equation (2.12), where γ_e denotes the so-called gyromagnetic ratio of an electron.

$$\nu = \frac{g_e * \mu_B * \vec{B}}{h} = \gamma_e \vec{B} \tag{2.12}$$

To observe intensive absorption it is required that different spin states are not equally populated, which fortunately is true. Mathematically the population difference of an arbitrary system can be described by a Boltzmann distribution, given in equation (2.13), where N is the number of spins being in the state indicated by the suffix.

$$\frac{N_\alpha}{N_\beta} = e^{-\frac{\Delta E}{k_B * T}} \qquad (2.13)$$

2.3 Basic Instrumentation

In this chapter a rough picture, which lacks deep technical insights, is given, to explain why an ESR signal looks like it does. Therefore especially those aspects of ESR instrumentation, which have an impact on the signal, other than disturbing it by drifting, will be pointed out. Figure 6 shows a schematic drawing of an arbitrary instrument. Usually the microwave radiation is kept constant, while the magnetic field is increased until the resonance condition (2.12) is satisfied.

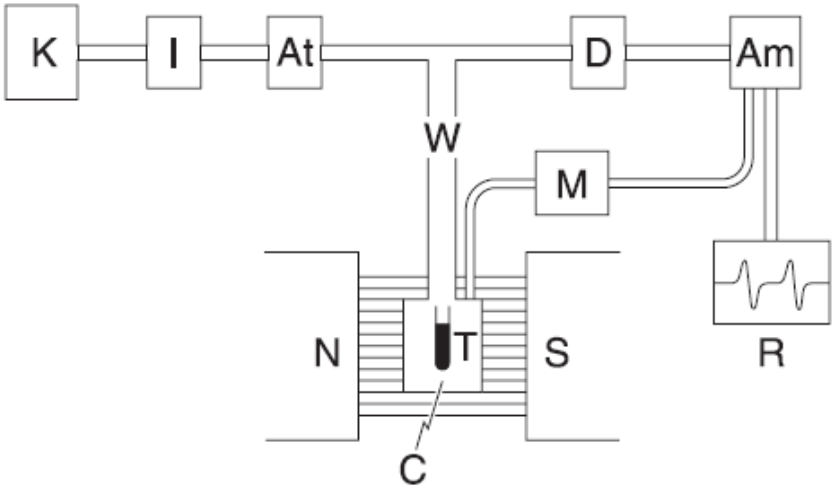

Figure 6: Schematic ESR instrument [8]

K denotes a Klystron, which has been the most common source of Microwave radiation, due to its ability to produce radiation with a relatively defined frequency in a rather small range. Usually they are operating at X band (≈ 9.5 GHz/ 3cm wavelength). Considering a g-factor of approximately 2 for organic radicals a resulting field of approximately 3400G is required to satisfy the resonance condition. The field is produced by an electromagnet where **N** and **S** denote his poles. Also, higher frequencies with higher corresponding field strengths are used, which is favourable because of the increasing population difference of spin states. In modern instruments the Gunndiode replaced the Klystron.

The waveguides **W** are designed to carry the microwave efficiently. Therefore their dimension matches the microwaves wavelength and they cannot be penetrated by it.

The ferrite isolator **I** protects the Klystron from being damaged by reflected microwave power.

The first part directly influencing the signal is the attenuator **At**, which regulates the power of the microwave before it hits the sample in a tube **T**. The amount of signal, which is quantified

through integration, is directly proportional to the adjusted power. This would not be valid if the absorption would be detected indirectly by transmission.

Actually the signal is detected by reflection from the cavity **C**. The microwave enters and leaves it from above, after being reflected at the cavity´s bottom. The microwave phase is adjusted, such that a standing wave forms which destructively interferes with itself, so that the overall power output is close to zero, which is favourable in terms of the recorded baseline. If this condition is achieved one speaks of critical coupling. Absorption of a sample disturbs this standing wave, so that more power is reflected, which is the signal detected at a detector **D**, a diode crystal e.g.

The role of the amplifier **Am** and the recorder **R** are self-explanatory.

In figure 6 the reference arm is not shown, which is in some instruments used to improve the signal to noise ratio, which is a function of the power hitting the detector. Due to the rather low power of the signal additional power must applied to reach optimal conditions. This is usually called the bias.

However, the greatest influence on the shape of ESR spectra has the modulation **M**, which is inter alia responsible for the detection of first derivative signals. Inside the cavity two field coils are placed, where an AC with a defined frequency (usually 100 kHz) is applied. The resulting oscillating magnetic field B_m has two effects. First of all it generates a signal with the same frequency as the AC which improves the signal to noise ratio tremendously if the detection system works frequency selectively. Secondly one records the first derivative of the absorption/reflection spectra because the instruments records the difference of the signal at the extreme values of the modulation frequency, as shown in figure 7. Moreover the amplitude of the modulation limits the resolution of the spectra. If the modulation amplitude is higher than the smallest distance between two signals, it will be recorded as one. However, the amount of signal is directly proportional to the modulation amplitude. Therefore so-called over modulation is sometimes required to get a signal at all.

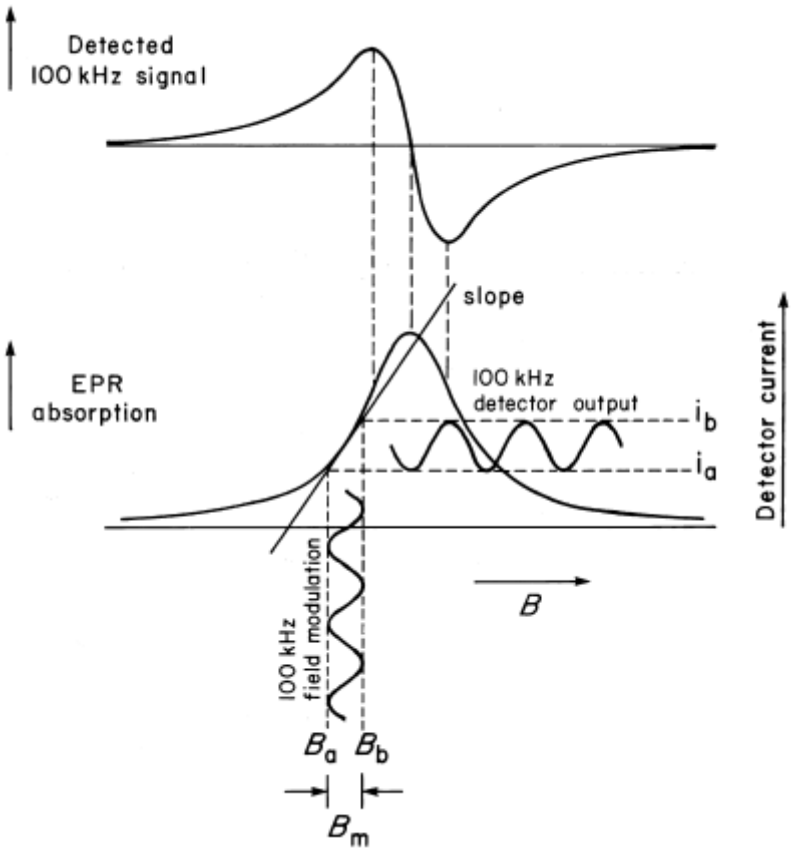

Figure 7: Influence of the modulation [8]

2.4 The ESR Spectrum

An ESR spectrum is simply the plot of the absorbed microwave power in arbitrary units versus the effective magnetic field strength. The line shape of a signal corresponds to either a Lorentzian, a Gaussian or any combined function. Equations (2.14) and (2.15) show the absorption A as a Lorentzian function, which is usually observed for organic radicals, and its first derivative; equations (2.16) and (2.17) show the same for a Gaussian function, which is sometimes observed for metal organic complexes. Here Γ denotes a peak´s half width at half height and B_r the field corresponding to the centre of the peak.

$$A = A_{max} \frac{\Gamma^2}{\Gamma^2 + (B - B_r)^2} \tag{2.14}$$

$$A' = -A_{max} \frac{2 * \Gamma^2 * (B - B_r)}{(\Gamma^2 + (B - B_r)^2)^2} \tag{2.15}$$

$$A = A_{max}\, exp\left[-\frac{\ln(2) * (B - B_r)^2}{\Gamma^2}\right] \tag{2.16}$$

$$A' = -A_{max}\left[\frac{2 * \ln(2) * (B - B_r)^2}{\Gamma^2}\right] exp\left[-\frac{\ln(2) * (B - B_r)^2}{\Gamma^2}\right] \quad (2.17)$$

An overview of the most important information contained in an ESR spectrum will be discussed here.

(A) The g-factor is similar to chemical shifts in NMR spectroscopy and identifies the type of paramagnetic species. It can be determined from the frequency used and field at the center of the spectrum via the resonance condition (2.12).

(B) If the first derivative spectrum is integrated twice one obtains an area, which is a measure for the amount of signal. This amount of signal corresponds to the whole absorbed/reflected microwave power P_A with a frequency, which arrives at the detector, described by equation (2.18). The new variables B_1 and ω will be discussed in chapter 2.6. The static magnetic susceptibility χ^0 is defined in equation (2.19), where N_V denotes the number of magnetic species per volume unit and κ is a dimensionless factor describing the medium.

$$P_A = \frac{\omega B_1^2}{\mu_0} \frac{\pi \chi^0 B_r}{(1 + \gamma_e^2 B_1^2 \tau_1 \tau_2)} A(\omega - \omega_B) \quad (2.18)$$

$$\chi^0 = \frac{\kappa g^2 \mu_B^2 \mu_0}{4 k_B} * \frac{N_V}{T} \sim \frac{C}{T} \quad (2.19)$$

Equations (2.18) and (2.19) indicate two experimentally proven effects on the amount of signal. First of all it decreases with temperature, which can be understood in terms of increasing thermal motion, which disturbs the orientation along the magnetic field. Secondly for a constant volume of a sample in solution it is directly proportional to the concentration of paramagnetic species, and vice versa. Therefore it can be used in quantitative analytics, where the method´s limitation to paramagnetic species turns out to be an advantage. Unfortunately the double integration is highly prone to noise, thus this method lacks reproducibility.

(C) Structural information is contained within the so-called hyperfine structure, which arises from the interaction of the magnetic moments induced by the electron spin with all nuclear spins present in the analyte. The nuclear spin behaves exactly as an electron spin in a magnetic field, but the magnetic moments $\vec{\mu}_n$ of the nuclear spin vector are significantly smaller, due to the higher mass. Moreover the nuclear spin quantum

number I can have values, which are multiples of ½, which leads to more magnetic quantum numbers m_I. Every spin state arising from the Zeeman splitting is distorted by the hyperfine interaction, thus additional spin states are produced dependent on m_s and m_I. Two effects determine the magnitude of the hyperfine interaction E_{hf} in terms of energy, as indicated by equation (2.20), where E_{dip} denotes the anisotropic dipolar interaction and E_{Fc} the so-called Fermi Contact Term.

$$E_{hf} = E_{dip} + E_{Fc} \qquad (2.20)$$

The symmetry of the orbital occupied by the free electron determines which contribution to E_{hf} is dominant. If the orbital has a symmetry different from an s-orbital the probability density of the electron is relatively far away from the nucleus. Therefore its magnetic moment can be approximated as a point dipole as it is drawn in figure 8.

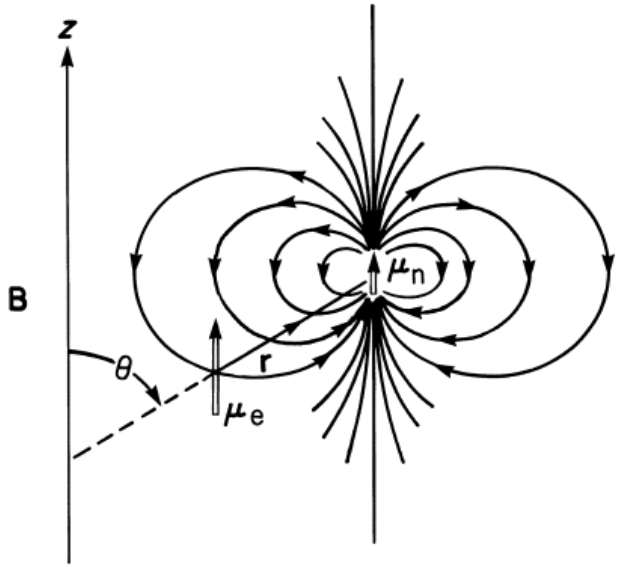

Figure 8: Dipolar interaction [8]

From this picture E_{dip} can be calculated by equation (2.21), where the anisotropy is indicated by the last factor dependent on the angle θ. Here μ_0 denotes the magnetic permeability of vacuum, μ_N the nuclear magneton and r the distance between the two dipoles.

$$E_{dip} = \frac{\mu_0 * g_e * g_n * \mu_B * \mu_N * m_s * m_I}{4\pi * r^3} * (3\cos^2\Theta - 1) \qquad (2.21)$$

The strongest dipolar interaction is found for θ being 0° or 180°, the smallest for θ being 90° or 270°. If the angle equals a value of 54.7° the dipolar interaction disappears. This is utilized in solid state magnetic resonance experiments in terms of the magic angle spinning. In solution the effect of dipolar interaction is usually not observed due to the Brownian motion. However, this motion is highly dependent on viscosity, therefore it can sometimes be observed in highly viscous solvents at low temperature.

If the orbital has s-symmetry the interaction becomes dependent on the probability density of the spin in the center of the nucleus ρ_s, where the magnetic moments are in close contact, thus it is isotropic. The mathematical expression for E_{Fc} is given in equation (2.22).

$$E_{Fc} = \frac{2}{3} * \mu_0 * g_e * g_n * \mu_B * \mu_N * m_s * m_I * \rho_s(0) \qquad (2.22)$$

The distance between two adjacent absorption lines, which correspond to spin states generated from hyperfine interaction with the same nucleus, is called hyperfine splitting constant. The expression for constant a_x in equation (2.21) is deviated from considering the hyperfine interaction in the resonance condition. From equation (2.23) it becomes obvious that a_x is only dependent on ρ_s. This is remarkable due to the fact that here a purely quantum mechanical property is directly proportional to an experimental quantity.

$$a_x = B_2 - B_1 = \frac{4\,E_{Fc}}{g_e * \mu_B} = \frac{2}{3} * \mu_0 * g_n * \mu_N * \rho_S(0) \qquad (2.23)$$

In summary the hyperfine interaction leads to new spin states, thus additional absorption lines can be observed, as it is depicted in figure 9.

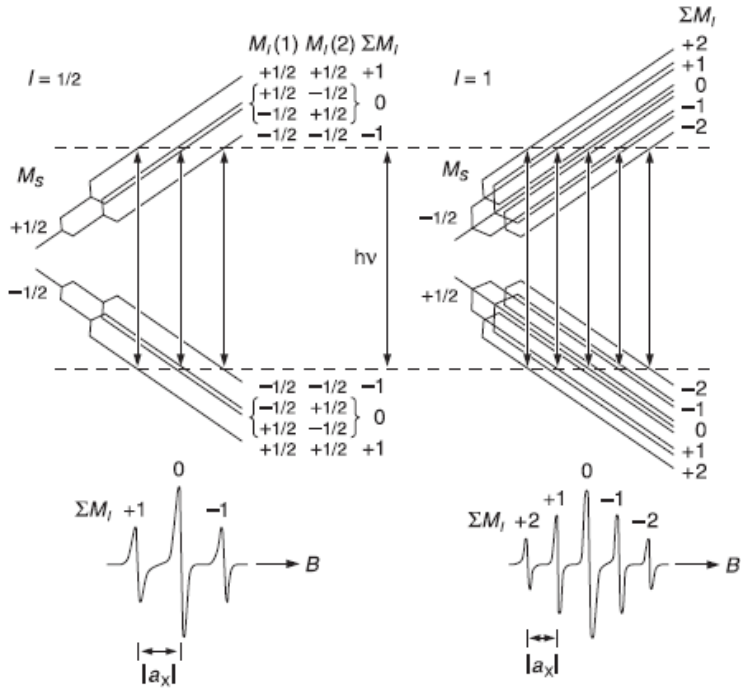

Figure 9: Hyperfine interaction for two equivalent nuclei with I = ½ (left) and I = 1 (right) [7]

The number of these so-called hyperfine lines coming from one nucleus is given by the multiplicity as well (chapter 2.2) where I instead of S is used for the calculation. If there are more nuclei present, one can obtain the overall number of lines N from equation (2.24), where n_i denotes the number of magnetically identical nuclei, meaning they can be transformed into each other by symmetry operations.

$$N = \prod_{i}^{k}(2n_i * I_i + 1) \qquad (2.24)$$

The intensity of each line is dependent on I and the number of magnetically identical nuclei, as shown in figure 10.

n =	I = 1/2							
0				1				
1			1		1			
2		1		2		1		
3	1		3		3		1	
4		1		4		6		4		1
5	1		5		10		10		5		1
6	1	6		15		20		15		6		1

I = 1									
			1						
		1		1		1			
	1		2		3		2		1
1		3		6		7		6		3		1
	4		10		16		19		16		10		4		1

n =	I = 3/2							
0				1				
1			1		1		1	
2	1		2		3		4		3		2		1

Figure 10: Scheme to determine the intensity of n hyperfine lines dependent on I [7]

The overall width of the spectrum W is calculated by equation (2.25)

$$W = \sum_{i}^{k} (2n_i * I_i * a_{x,i}) \tag{2.25}$$

(D) The dynamic information is usually obtained from the line width, which will be discussed further in chapters 2.5 - 2.7. An approximation for the half width at half height Γ is given in equation (2.26) in units of a magnetic field, which is valid for continuous wave experiments. Here a Lorentzian lineshape has been assumed. The variable τ_2 is defined in chapter 2.5; a more detailed description of ΔB is given in chapter 2.6 in equation (2.67).

$$\Delta B = \frac{1}{\gamma_e * \tau_2} \tag{2.26}$$

Alternatively it can be measured from the maxima to the minima of one line in the first derivative spectrum. This peak to peak line width ΔB_{pp} is related to the half width at half height for a Lorentzian function according to equation (2.27).

$$\Delta B_{pp} = \frac{2}{\sqrt{3}} \Gamma \tag{2.27}$$

2.5 Line Broadening and Relaxation Processes

ESR lines are naturally broadened due to the Heisenberg uncertainty principle, which is shown in equation (2.28) for the uncertainty in energy ΔE and time Δt.

$$\Delta E * \Delta t \geq \frac{h}{2\pi} \tag{2.28}$$

Considering the resonance condition and the definition of radiant energy one can rewrite equation (2.28) in the form of equation (2.29). Here the uncertainty of ΔB can be interpreted as line width.

$$\gamma_e \Delta B * \Delta t \geq \frac{1}{2\pi} \tag{2.29}$$

The magnitude of the line width is therefore indirectly proportional to the uncertainty in time. It can be interpreted as the lifetime of a spin state τ_{ss}, which has been excited by absorption. This lifetime can be determined from equation (2.30), where k_i is the first order kinetic rate constant (inverse of the lifetime) of every process, which annihilates the excited state.

$$\frac{1}{\Delta t} = \frac{1}{\tau_{ss}} = \sum_{i=1}^{n} \frac{1}{\tau_i} = \sum_{i=1}^{n} k_i \qquad (2.30)$$

In general here are two different possibilities of the annihilation of an excited state. On one hand the system can be transformed into something different, by a chemical reaction e.g., on the other hand the excited state can undergo relaxation.

For further purposes relaxation is defined as every process, which transfers an energetically excited state back to the energetic ground state. In this chapter relaxation processes are discussed in general, however, a mathematical description for an experimentally relevant system is elaborated in chapter (2.6).

First of all one has to distinguish between two fundamentally different types of relaxation, which are called longitudinal and transversal relaxation. The former is a thermal process, the latter relates to chemical dynamics.

(A) The rate of longitudinal relaxation is usually associated with a lifetime τ_1. Considering the picture in figure 4, one realizes that during absorption the spin of an electron has to invert its orientation. Thus the opposite process is called longitudinal relaxation. During this relaxation process the spin-system, a radical e.g., has to get rid of the excess in internal energy, which is done by distributing it to the surrounding "lattice". Thus the term spin-lattice relaxation is used alternatively. It is described by an exponential decay, given in equation (2.31), where ΔU_x denotes the internal energy at a moment with t = x.

$$\Delta U_t = \Delta U_0 * e^{\frac{-(t - t_0)}{\tau_1}} \qquad (2.31)$$

For an arbitrary sample, which contains a large amount of spins, the overall internal energy is the sum of every individual spin state. Hence it is closely related to the difference in population ΔN. Therefore equation (2.31) can be expressed in terms of ΔN instead of ΔU. This is given in equation (2.32), where ΔN_{eq} denotes the population difference for the system in thermal equilibrium before excitation, and ΔN_{ex} the one after excitation.

$$\Delta N = \Delta N_{ex} + \left(\Delta N_{eq} - \Delta N_{ex}\right) * \left(1 - e^{-\frac{(t - t_0)}{\tau_1}}\right) \qquad (2.32)$$

Due to the fact that constant microwave irradiation would lead to the formation of a new thermal equilibrium, τ_1 can only be obtained from a pulsed ESR experiment, which is called saturation recovery.

(B) The rate of transversal relaxation is usually associated with a lifetime τ_2. This summarizes a variety of isoenergetic processes, such as Heisenberg exchange or electron self-exchange. The former describes the exchange of information about the orientation, the latter is discussed in part one of this thesis. It is important to point out, that both of these processes are related to diffusion, which makes them highly sensitive to temperature. [32]

The term transversal is used because the overall orientation in x- and y-direction of a distinct spin state is altered, but not the population difference. Thus the rate of these processes must be independent of the population difference ΔN, hence it can be obtained from analysing line widths in continuous wave ESR experiments. This is discussed in chapter 2.7. Another possibility to measure τ_2 is the so called spin echo experiment in pulsed ESR.

If one influences the rate of any diffusion dependent transversal relaxation process by increasing the concentration of the paramagnetic species or adding any kind of quencher, the shape and position of lines is altered. Mathematical descriptions of these proportions are discussed in chapter 2.7. These so-called line broadening experiments are especially useful in the study of thermo neutral reactions, such as electron self-exchange. An overview of the possibilities and limitations of this method in respect to electron self-exchange is given in a review article by G. Grampp. [33]

Unfortunately the line width is influenced by other factors as well, which complicate the experimental determination of kinetic information related to τ_2. Especially inhomogeneous line broadening is problematic.

The first point one has to consider unresolved hyperfine lines, which arise either from Fermi contact or dipolar interactions. If the modulation amplitude is larger than the hyperfine coupling constants one detects an envelope of a multitude of lines. Dependent on the hyperfine structure of the analyte the line width of the envelopes can additionally differ within the spectrum. These problems can be solved by a good knowledge about the hyperfine

coupling constants from either quantum chemical calculations or ENDOR experiments. The latter are described in part three of this thesis.

Moreover an inhomogeneous external magnetic field, can lead to inhomogeneous line broadening. This inhomogeneity can also arise from other fixed paramagnetic centres, which interact as dipoles with the spin of the analyte.

Also statistics play a role in inhomogeneous line broadening. Usually the central lines of a spectrum are less broadened than the other ones. This is related to the fact that the central line corresponds to a larger ensemble of equivalent spin states, hence they have a higher probability of encountering an equivalent spin state. These collisions cause no alteration of τ_2, hence there is no detectable influence on the lines.

2.6 The Bloch Model

The Bloch Model treats relaxation in a simple picture from classical physics, which is working quite well for diluted systems. The concrete behaviour of an individual spin and effects like the attenuation of radiation by the medium or the magnetization of emitted photons are not included.

In chapter 2.5 the influence of relaxation on the experimentally observed line width was mentioned. Due to the fact that a real sample contains a huge number of unpaired electron spins, which constantly change their spin state by excitation, relaxation and/or chemical transformations, a macroscopic description of the system as a whole is desired in order to interpret these observations properly because the observation must be an average of all processes going on. Therefore the magnetization $\overrightarrow{\mathrm{M}}$ is introduced as macroscopic quantity in equation (2.33), which is always normalized to the volume V of the sample.

$$\vec{M} = \frac{1}{V} * \sum_{i=1}^{n} \vec{\mu}_e \qquad (2.33)$$

Alternatively the magnetization can be related to the applied field. For an electron this is expressed in equation (2.34), where χ_m denotes the rationalized volume magnetic susceptibility.

$$\vec{M} = \frac{\chi_m}{\kappa * \mu_0} * \vec{B} \qquad (2.34)$$

Relaxation causes the change of a spins individual orientation over time, thus it is nothing but an alteration of $\vec{M}$ over time. Therefore the time dependence of $\vec{M}$ must be considered first, which will be done in a simple vector model. In solution the magnetic moments of every spin are oriented randomly in all directions before the magnetic field is applied, hence the magnitude of $\vec{M}$ is approximately zero. When the magnetic field is switched on, the spins experience $\vec{B}$, which leads to a force that tries to align them parallel to the field lines. This orientation leads to an exponential rise of the vector $\vec{M}$, which is illustrated in figure 11 for its z-component.

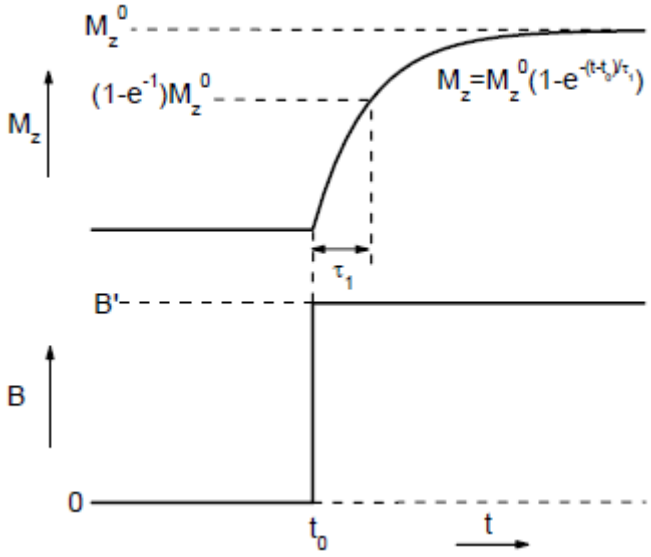

Figure 11: Behavior of $\vec{M}$ when the magnetic field is applied [8]

The resulting rotation, with the Larmor frequency ω_B given by equation (2.35), induces a centrifugal force in the opposite direction that leads to a stable precission for every spin vector corresponding an equilibrium of the opposed forces.

$$\omega_B = -\gamma_e * B \qquad (2.35)$$

Therefore the magnetization also precesses with a frequency ω_0, which is the average of all values for ω_B, around the field lines. In terms of classical physics the time dependence of $\vec{M}$ can be expressed by a change of angular momentum, which is formulated for the magnetization in equation (2.36). From the analytical solution of (2.36) one can obtain the Larmor frequency.

$$\frac{d\vec{M}}{dt} = \gamma_e * \vec{M} \times \vec{B} \tag{2.36}$$

With $\vec{B}$ pointing in the z-direction, the x-, y- and z-components in equations (2.37) – (2.39) are obtained from computing this vector product.

$$\frac{dM_x}{dt} = \gamma_e * B * M_y \tag{2.37}$$

$$\frac{dM_y}{dt} = -\gamma_e * B * M_x \tag{2.38}$$

$$\frac{dM_z}{dt} = 0 \tag{2.39}$$

Now the longitudinal and transversal relaxation discussed in chapter 2.5 are introduced in terms of their contributions τ_1 and τ_2 to the overall lifetime. This is shown below in equations (2.40) – (2.42).

$$\frac{dM_x}{dt} = \gamma_e * B * M_y - \frac{M_x}{\tau_2} \tag{2.40}$$

$$\frac{dM_y}{dt} = -\gamma_e * B * M_x - \frac{M_y}{\tau_2} \tag{2.41}$$

$$\frac{dM_z}{dt} = \frac{M_z^0 - M_z}{\tau_1} \tag{2.42}$$

The problem with the picture so far is that relaxation can only occur after excitation. In ESR this is done by irradiation with a micro wave perpendicular to the magnetic field. For obvious reasons only the magnetic part of this wave is important. This is described by an additional field $\overrightarrow{B_1}$, which oscillates with the frequency ω, given in equations (2.43) – (2.45).

$$B_{1,x} = B_1 * \cos(\omega t) \tag{2.43}$$

$$B_{1,y} = B_1 * \sin(\omega t) \tag{2.44}$$

$$B_{1,z} = 0 \tag{2.45}$$

Therefore the actual field, which is responsible for $\vec{M}$ is resulting from B and B_1 simultaneously. In absence of relaxation the formulation in equation (2.46) would be valid.

$$\frac{d\vec{M}}{dt} = \gamma_e * \vec{M} \times \left(\vec{B} + \vec{B}_1\right) \tag{2.46}$$

In equations (2.47) – (2.49), which are the famous Bloch equations, relaxation is considered.

$$\frac{dM_x}{dt} = \gamma_e * [B * M_y - B_1 * \sin(\omega t) * M_z] - \frac{M_x}{\tau_2} \tag{2.47}$$

$$\frac{dM_y}{dt} = -\gamma_e * [B * M_x - B_1 * \cos(\omega t) * M_z] - \frac{M_y}{\tau_2} \quad (2.48)$$

$$\frac{dM_z}{dt} = \gamma_e * [B_1 * \sin(\omega * t) * M_x - B_1 * \cos(\omega t) * M_y] - \frac{M_z^0 - M_z}{\tau_1} \quad (2.49)$$

To solve this system of coupled differential equations Bloch transformed them in a new coordinate frame, which rotates with ω around the z-axis. The new x-axis x_ϕ always points in the direction of B_1, through a rotation by the angle ϕ, which is measured between the new and the old x-axis. Thus the equations, which are given in equations (2.50) – (2.52), get significantly simpler.

$$\frac{dM_{x,\phi}}{dt} = -(\omega_B - \omega) * M_{y,\phi} - \frac{M_{x,\phi}}{\tau_2} \quad (2.50)$$

$$\frac{dM_{y,\phi}}{dt} = (\omega_B - \omega) * M_{x,\phi} - \frac{M_{y,\phi}}{\tau_2} \quad (2.51)$$

$$\frac{dM_z}{dt} = -\gamma_e * B_1 * M_{y,\phi} - \frac{M_z^0 - M_z}{\tau_1} \quad (2.52)$$

The appropriate set of steady-state solutions is displayed in equations (2.53) – (2.55).

$$M_{x,\phi} = -M_z^0 * \frac{\gamma_e * B_1 * (\omega_B - \omega) * \tau_2^2}{1 + (\omega_B - \omega)^2 * \tau_2^2 + \gamma_e^2 * B_1^2 * \tau_1 * \tau_2} \quad (2.53)$$

$$M_{y,\phi} = M_z^0 * \frac{\gamma_e * B_1 * \tau_2}{1 + (\omega_B - \omega)^2 * \tau_2^2 + \gamma_e^2 * B_1^2 * \tau_1 * \tau_2} \quad (2.54)$$

$$M_z = M_z^0 * \frac{1 + (\omega_B - \omega)^2 * \tau_2^2}{1 + (\omega_B - \omega)^2 * \tau_2^2 + \gamma_e^2 * B_1^2 * \tau_1 * \tau_2} \quad (2.55)$$

A closer look at these equations shows that saturation is included, due to the quadratic dependence on B_1 of the third term in denominator. In literature this term is sometimes called the (power)-saturation term. If B_1 is small, which is usually the case for an ESR experiment, the saturation term becomes negligible, and hence the influence of τ_1 disappears. In conclusion the line width of a continuous wave ESR experiment is virtually independent of τ_1.

The solutions of the Bloch equations are not absolutely accurate in describing an ESR experiment. Usually $\vec{B}_1$ is applied linearly in the x-direction. Therefore equation (2.56) is used instead of equation (2.42); the x- and y-components of $\vec{B}_1$ are equal to zero.

$$B_{1,x} = 2 * B_1 * \cos(\omega t) \quad (2.56)$$

For positive values of ω one can express $\vec{B}_1$ as sum of two fields of equal magnitude, which rotate in opposite directions. A mathematical expression is given in equation (2.57).

$$\vec{B}_1 = \vec{B}_{1,+} + \vec{B}_{1,-} = B_1 * \left[\begin{pmatrix} \cos(\omega t) \\ \sin(\omega t) \\ 0 \end{pmatrix} + \begin{pmatrix} \cos(\omega t) \\ -\sin(\omega t) \\ 0 \end{pmatrix} \right] \qquad (2.57)$$

The component $\vec{B}_{1,+}$ rotates per definition in the same direction as $\vec{M}$. Therefore the term (ω_B - ω) in equations (2.53) – (2.55) gets rather small and the effect on $\vec{M}$ is considerable. The opposite is true for the component $\vec{B}_{1,-}$, which means that only fifty percent of the energy density of the radiation is effectively inducing transitions.

The influence of B_1 on the magnetization can alternatively be expressed in terms of susceptibilities. Therefore two dynamic susceptibilities χ´, representing the dispersion, and χ´´, representing the power absorption P_A, are defined in equations (2.58) and (2.59). The definition of χ^0 has already been defined in chapter 2.4 as equation (2.19).

$$\chi' = \chi^0 * \frac{\omega_B * (\omega_B - \omega) * \tau_2^2}{1 + (\omega_B - \omega)^2 * \tau_2^2 + \gamma_e^2 * B_1^2 * \tau_1 * \tau_2} \qquad (2.58)$$

$$\chi'' = \chi^0 * \frac{\omega_B * \tau_2}{1 + (\omega_B - \omega)^2 * \tau_2^2 + \gamma_e^2 * B_1^2 * \tau_1 * \tau_2} = \frac{\chi'}{(\omega_B - \omega) * \tau_2} \qquad (2.59)$$

Inserting equations (2.58) and (2.59) in equations (2.53) – (2.55), one yields a simpler expression of the steady state solutions of the Bloch equations, which are displayed in equations (2.60) – (2.62).

$$M_{x,\phi} = \frac{\kappa \mu_0 \chi'}{B_1} \qquad (2.60)$$

$$M_{y,\phi} = \frac{\kappa \mu_0 \chi''}{B_1} \qquad (2.61)$$

$$M_z = \frac{\kappa \mu_0 \chi^0}{B_1} \qquad (2.62)$$

This representation leads to one limitation of the Bloch model. Assuming the external field being equal to zero, the Larmor frequency would be zero, thus the susceptibilities would vanish, which is physically impossible.

The expression for the dynamic susceptibility χ´´ in equation (2.59) can be rewritten to equation (2.63). Its half width at half height Γ is given in equation (2.64).

$$\chi'' = \chi^0 B_r * \frac{1}{\Gamma^2 + (\omega - \omega_B)^2} \tag{2.63}$$

$$\Gamma = \frac{1}{\tau_2} * \sqrt{1 + \gamma_e^2 * B_1^2 * \tau_1 * \tau_2} \tag{2.64}$$

As already mentioned χ'' is related to the power absorption P_A, which can be expressed by equation (2.65).

$$P_A = \frac{\omega B_1^2 \chi''}{\mu_0} \tag{2.65}$$

The general expression for P_A, which is given in chapter 2.4 as equation (2.18), is obtained from combining equations (2.63) and (2.65). Therefore equation (2.63) is rewritten to a general Lorentz function, due the general relevance to organic radicals of this presentation.

To convert the power from units of frequency to magnetic field one has to multiply with the gyromagnetic ratio according to the resonance condition. Thus the half width at half height in the frequency domain from equation (2.64) results in equation (2.66) in the magnetic field domain, where it is called ΔB.

$$\Delta \mathrm{B} = \frac{1}{|\gamma_e| \tau_2} * \sqrt{1 + \gamma_e^2 * B_1^2 * \tau_1 * \tau_2} \tag{2.66}$$

Assuming non saturated conditions equation (2.66) reduces to the simple expression given in equation (2.26).

2.7 Line Broadening Experiments and Dynamic Lineshape Effects

In chapter 2.5 the basic idea of a concentration dependent line broadening experiments in continuous wave ESR to determine kinetics of transversal relaxation processes has been mentioned. This experiment is discussed in respect to electron self-exchange; however, the same considerations apply to Heisenberg exchange.

A detailed discussion of the kinetics of ET and electron self-exchange is given in chapter 1.9 in the first part of this thesis. There k_{obs} was introduced as the experimentally observed rate constant, where a general theoretical expression had been derived in equation (1.21). Equation (2.67) relates k_{obs} to the investigated process, where the suffix x and y denote different nuclear spin configurations.

$$A_x + A_y^- \xrightarrow{k_{obs}} A_x^- + A_y \tag{2.67}$$

The experiment is set up to satisfy the assumption that the line broadening only corresponds to electron self-exchange, which is indicated by equation (2.69) In chapter 2.6 it has already been discussed why longitudinal relaxation is negligible in continuous wave experiments. Other transversal relaxation processes, such as Heisenberg exchange, broaden the lines as well. Therefore the concentration of the paramagnetic species is kept constant, and this effect is considered to be part of the natural line width, which will be discussed in the following. The concentration of the diamagnetic species [A], is varied, where [A] ≥ [A^-].

$$k_{obs} = \frac{1}{\tau_{ss}\,[A]} \qquad (2.68)$$

The overall line width ΔB can be formulated as the sum of the natural line width ΔB^0 plus the additional line broadening due to electron spin exchange. This is expressed by equation (2.69), in the commonly used first derivative ESR-mode. In an ideal system the natural line width should arise from the Heisenberg uncertainty principle only, however, in every experiments other transversal relaxation processes are present. If their influence can be kept constant, the just add to the natural line width.

$$\Delta B = \frac{\sqrt{3}}{2}\,\Delta B_{pp}^{0} + \frac{(1-p_i)}{|\tau_{ss}\gamma_e|} \qquad (2.69)$$

There p_i denotes a statistical factor. This factor considers the possibility of a reaction between two species with equivalent nuclear configurations x and y, which cannot be detected. It is defined as the degeneration of the i^{th} line over the total number of spin configurations.

Combining equations (2.68) and (2.69) yields a linear relation between k_{obs} and the change in line width, given in equation (2.70).

$$k_{obs} = \frac{\sqrt{3}\pi|\gamma_e|(\Delta B_{pp} - \Delta B_{pp}^{0})}{(1-p_i)[A]} \qquad (2.70)$$

Equation (2.70) predicts that a plot of $(\Delta \mathrm{B_{pp}} - \Delta \mathrm{B_{pp}^0})$ versus [A] gives a straight line with a slope proportional to k_{obs} and an intercept equal to $\Delta \mathrm{B_{pp}^0}$.

Experiments showed that this is only valid in the so-called slow exchange region. At certain concentration [A] the outer lines begin to shift towards the centre, which can be understood by the limitation in time resolution of the instrument compared to the reaction rate. This is the so-called intermediate region. Further increase in [A] the spectrum collapses to one single line, which is the so-called fast region. Expressions for k_{obs} in these regions are given in

literature. [33] This dynamic lineshape effect is illustrated in figure 12. It can be derived from the Bloch model, by introducing an additional dynamic part, which is usually solved computationally.

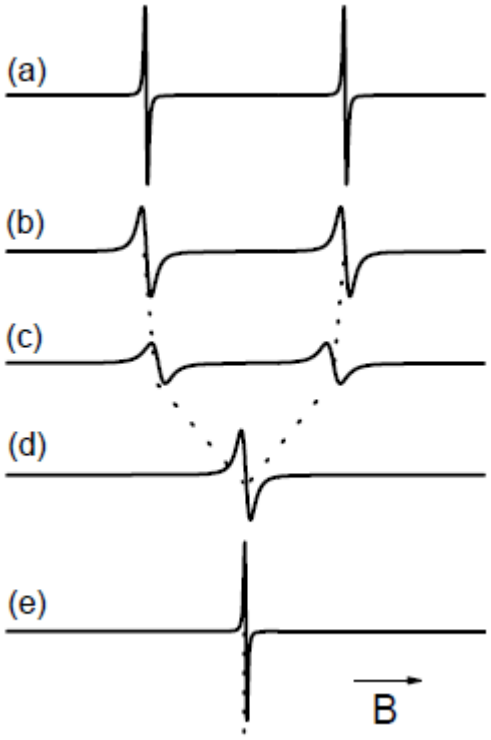

Figure 12: Synthetic line broadening experiment [8]

a) slow limit (no exchange happening)

b) slow region following equation (2.71)

c) intermediate region showing line shifts

d) fast region

e) fast limit

Part 3: Electron Nuclear Double Resonance

3.1 Introduction

To obtain accurate values for line widths the knowledge of hyperfine splitting constants is essential. In chapter 2.4 equation (2.24) is introduced to calculate the number of lines of an ESR spectrum. A general expression for this number is given in equation (2.24), which describes a product of the number and spin of all magnetically active but chemically different nuclei. Intuitively this is explained due to the fact that one records the signal of one single electron spin interacting with all nuclear spins. These quite complex spectra for not too complicated molecules with many overlapping lines, which makes it impossible to obtain exact values for hyperfine splitting constants.

Therefore it seems preferable to measure signals from every type of nucleus k with a spin quantum number I_k and his interaction with the electron spin individually to determine hyperfine splitting constants, which could theoretically be done by NMR experiments. Then the number of lines n is described by equation (3.1), thus it increases additively. Therefore this kind of spectrum is considerably simpler to analyze.

$$n = 2 * (2S + 1) * \sum_{k=1}^{n} I_k \qquad (3.1)$$

Unfortunately NMR detection is less sensitive and has further problems with paramagnetic species. This problem has been overcome with the Electron Nuclear Double Resonance (ENDOR) experiment, which was discovered in 1956 by G. Feher. [31] In principle ENDOR uses an ESR instrument to indirectly detect NMR transitions. Nowadays this type of experiment is still the only method to experimentally determine hyperfine splitting constants from unresolved ESR spectra. Further it can be used to identify an interacting nucleus.

3.2 Fundamentals of ENDOR

The basic theoretical concept of an ENDOR experiment is illustrated in figure 13. This picture considers the interaction of an electron spin with a single nucleus with I = ½. This leads to four different spin states, which are drawn as boxes and named 1-4. The coloration of these boxes corresponds to the population of this spin state. The lines connecting the boxes illustrate transitions, where T_{1e} denotes common ESR transitions and T_{1n} NMR transitions respectively. T_x and T_{xx} denote so-called cross-relaxations.

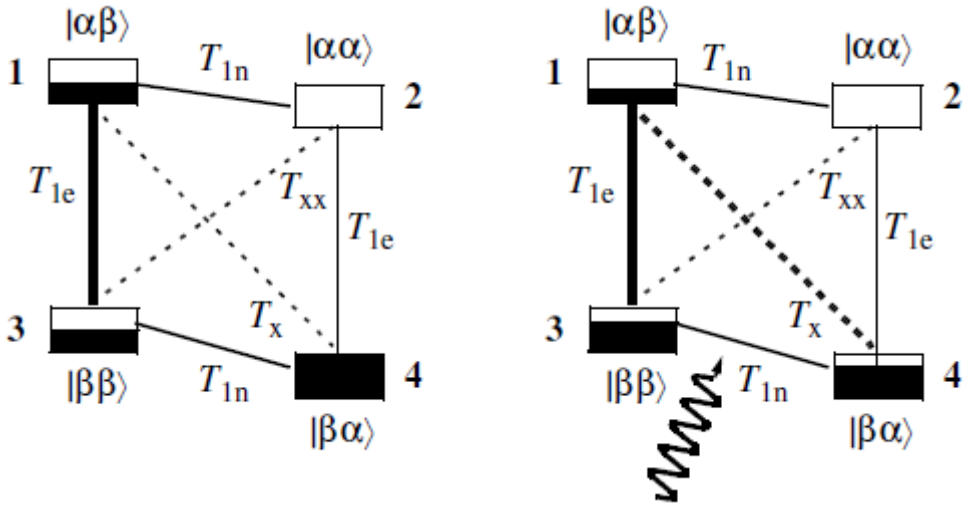

Figure 13: Two steps of an ENDOR experiment [34]

The energy E of these spin states is dependent on the quantum numbers m_s and m_I. A general expression is given in equation (3.2), where the electron Zeeman part, displayed as the first term is the dominant. The second term accounts for the nuclear Zeeman interaction, and the third is the electron-nucleus interaction, dependent on the hyperfine splitting constant A.

$$E = g\mu_B B m_s - g\mu_N B m_I + h * A * m_s * m_I \qquad (3.2)$$

Considering the resonance condition one can rewrite equation (3.2) in terms of transition frequencies ν, given in equation (3.3).

$$E = (\nu_E m_s - \nu_N m_I + A * m_s * m_I) * h \qquad (3.3)$$

First of all a normal ESR spectrum is recorded. Then the field is set to one specific ESR transition and the microwave power is increased. On the left picture in figure 13 the transition from 3 → 1 has already been saturated by microwave power, according to the saturation condition given in equation (3.4), which can be derived from the saturation term in equations (2.52) – (2.54) in chapter 2.6.

$$\omega_{mw}^2 = \gamma_e^2 * B_1^2 \; > \; \frac{1}{\tau_1 * \tau_2} \qquad (3.4)$$

When the rate of absorption is higher than the one of relaxation an equal population of spin state 1 and 3 is established and no further absorption can occur, thus the signal disappears as long as the microwave frequency is kept constant. Then high power radio frequency is scanned through the cavity. If this frequency matches at any point the energy difference of spin state 3 and 4, this transition can be saturated if the condition in equation (3.5) is fulfilled.

$$\omega_{rf}^2 > \frac{1}{\tau_x * \tau_{xx}} \tag{3.5}$$

If this is the case an equal distribution between spin state 4 and 3 is established, which ends the saturated condition for transition 3 → 1. In other words, the rate of relaxation from spin state 1 to 3 is now increased by the NMR transition. The new relaxation rate considering the NMR transition is related to a reduced lifetime τ_{rf}, given in equation (3.6).

$$\tau_{rf} = \frac{(\tau_1 * \tau_x)}{(\tau_1 + \tau_x)} \tag{3.6}$$

Hence the ESR line reappears, when the NMR transition occurs, which is the so-called ENDOR signal.

In order to obtain a stable ENDOR signal τ_x must be smaller τ_1. Both of these relaxation processes are exergonic, thus dependent on temperature. For the discussion here it is just mentioned that this temperature dependence is opposite for both, however, always related to the rotational correlation time τ_R, which is given in equation (3.7). In a simple picture V_{eff} can be described as a sphere with a radius given by the average one of a molecule.

$$\tau_R = V_{eff} * \frac{\eta}{k_B T} \tag{3.7}$$

Therefore fine tuning of the temperature and solvent is required to obtain an intense and stable ENDOR signal, which cannot be found for every radical.

3.3 The ENDOR Spectrum

The ENDOR Spectrum is a plot of microwave absorption/reflection in arbitrary units versus the radio frequency, which is usually measured in MHz.

Considering the NMR section rules ($\Delta m_I = \pm 1$) one can derive a general expression for the detected resonance frequencies ν_{NMR} from the difference in energy of two relevant spin states, given in equation (3.3), which is displayed in equation (3.8).

$$\nu_{NMR} = |-\nu_N + m_s * A| \tag{3.8}$$

This means that for a normal organic radical with one unpaired electron whith $m_s = \pm ½$ two lines for every type of nucleus are detected, which are separated exactly by the hyperfine coupling constant a. To get useful values for ESR one just has to convert the distance between the two ENDOR lines from MHz to units of magnetic field units. This relation is displayed in equation (3.9).

$$a\,[G] = 2.8025 * a\,[MHz] \qquad (3.9)$$

Equation (3.8) indicates further that the center of every doublet corresponds to the free nuclear frequency ν_N, which could be used to identify the type nucleus. Unfortunately these are so similar at the low fields used in ESR that the ENDOR spectrum usually appears around the same center.

In chapter 3.2 the relation of the ENDOR signal intensity to τ_{rf} was explained, hence it is not corresponding to the amount of equivalent nuclei, as it is in common NMR spectroscopy.

Part 4: Experimental

4.1 Introduction

Fukuzumi et al published [2] temperature dependent rate constants for the electron self-exchange of ZnTPP and Zn(tBu)PP and their corresponding radical cation in acetonitrile, dichloromethane and toluene. They obtained these rate constants from ESR line broadening experiments, however, no series of spectra of such an experiment is available in their publication or the supplemental information. From these rate constants he calculated activation barriers, which are described as being relatively small and for the Zn(t-Bu)PP in toluene even negative. This unusual result was explained by the experimental observation of increasing line width with decreasing temperature. This behaviour has been observed for ZnTPP in MeCN as well, even though they did not calculate a negative activation barrier for this system. Thus this effect, which can arise from other dynamics, such as dipolar interactions, cannot be attributed to electron self-exchange only, hence this result of Fukuzumi et al is questionable.

Further, there are certain issues concerning solubility. ZnTPP is not quantitatively soluble in acetonitrile in the concentrations given in the publication, and the Ru-(III)-complex, which they used as oxidizing agent, turned out to be insoluble in toluene in the given concentration. Optimizing the system yielded various ways to generate the radical chemically in different solvents with similar polarity. Further, certain problems related to the rate of the oxidation itself, the long term stability of the radical and additional chemical transformations appeared. Therefore the oxidation was finally performed electrochemically in a flow apparatus, which is described in chapter 4.3.

The recorded spectra in this thesis did not correspond to the hyperfine coupling constants from the publication, which turned out to be at least 25% larger. Therefore ENDOR experiments have been performed, which gave hyperfine coupling constants that corresponded nicely to our measured spectra and the first one ever published for the ZnTPP radical cation. [37]

A closer look on the theory provided in the article of Fukuzumi et al shows additional discrepancies. On the one hand slow exchange has been assumed to obtain values of k_{obs}. Usually this can only be assumed without further proving, if one can resolve the hyperfine

structure, which is not the case. On the other hand the correction for diffusion, which has been used to determine values of k_{ET}, is not considered to be valid for electron self-exchange any more. This has already been mentioned in chapter 1.9, where the proper correction can be found.

Also it is important to point out that the utilized double zeta set of base functions for the quantum chemical calculations, which were used to support his assumptions, is relatively small and prone to errors. Therefore it is not used any more for this kind of problems.

4.2 Chemicals

All solvents that were used are listed in table 1. The ones used for ESR measurements were dried over a molecular sieve, distilled and stored under nitrogen atmosphere. On the same day as measurement was performed, a small amount was degassed by bubbling nitrogen through the solvent.

Solvent	Producer	Details
Acetonitrile (MeCN)	Sigma Aldrich	99.8% anhydrous
Butyronitrile (PrCN)	Alfa Aesar	99%
Chloroform (CF)	Fluka	puriss p.a.
1,2-Dichlorobenzene (oDCB)	RdH	99%
Ethyl acetate (EE)	Roth	99.9% rotisolv HPLC
n-Heptane	Roth	95% rorisol HPLC
Hexafluoro-2-propanol	Aldrich	99,8%
Methylene chloride (DCM)	Roth	99.8% rotidry
Toluene	Fluka	99% purum

Table 1: Solvents

The relevant information about all the oxidizing agents, which were purchased are listed in table 2.

Oxidizing Agent	Producer	Details
Ammonium-Cerium(IV)-nitrate	RdH	99% p.a.
Benzoyl peroxide (DBPO)	Fluka	97% purum
(Bis(trifluoracetoxy)iod)benzene	Aldrich	97%
Tris(4-bromophenyl)ammonium hexachloridoantimonate (Magic Blue)	Fluka	97% purum
Silver perchlorate	Fluka	97% purum

Table 2: Oxidizing agents

Additionally Ru-(III)-bipy$_3$(PF$_6$)$_3$ (bipy = 2,2-bipyridin) was used as oxidizing agent, which had to be synthesized, which was done similar to the literature. [2] Therefore Ru-(II)-bipy$_3$Cl$_2$ (Aldrich 99.99%) was dissolved in 10 V% H_2SO_4. An excess of insoluble Lead-(IV)-oxide (Fluka

98% puriss. p.a.) was added under permanent stirring. After a few seconds the orange solution turned green. The reaction mixture was stirred for 2h at room temperature, the solid lead-(IV)-oxide was removed with a folded filter. From the generated Ru-(III)-complex the final product was precipitated as a fine green powder by adding a slight excess of solid NH_4PF_6. (Fluka 99% purum) The product was obtained by a filtration, washed three times with distilled water and dried over P_2O_5 in vacuum.

The last oxidizing agent was nitrosyl-perchlorate, which had been synthesized according to literature. [35] It was stored in a brown flask in the fridge; hence it had to be dried again on a clay plate over P_2O_5 in vacuum for several days, before it could be used.

ZnTPP was synthesized from zinc-(II)-chloride (Merck 98% p.a.) and 5,10,15,20-tetraphenyl-21H,23H-porphyrine (Sigma Aldrich 99%) according to literature. [36] The reaction was monitored via TLC on silica gel 60 with chloroform: n-heptane = 1:3 as mobile phase. The Rf-values are 0,147 for ZnTPP and 0,265 for TPP, which were detected in UV light. The remaining zinc salt was removed quantitatively by column chromatography with chloroform as mobile and neutral aluminium oxide, which had been dried in the oven over night, as stationary phase. To verify the purity of the compound a ^{1}H-NMR spectrum in $CDCl_3$ was recorded, which is discussed in chapter 4.5.

The supporting electrolyte for electrochemical measurements was tetrabutylammonium tetrafluoroborate, (Fluka pure) which had been dried at 80°C in the high vacuum. It was stored under nitrogen atmosphere.

4.3 Instrumentation

All ESR measurements were performed with an ELEXSYS E-500 spectrometer from Bruker at X-band with a modulation frequency of 100 kHz.

CW-ESR measurements of chemically oxidized samples were performed with the special cylindrical HS-W10010 resonator. Additionally a thermo coupling unit can be attached, where temperature is regulated with a stream of nitrogen.

CW-ESR measurements of electrochemically oxidized samples were performed in the flow apparatus, which is shown in figure 14.

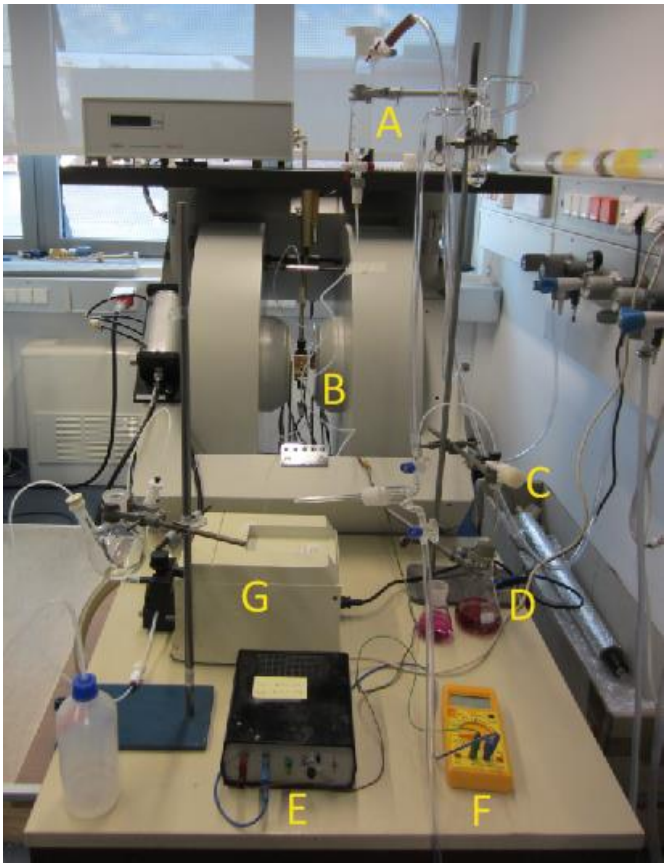

Figure 14: Flow apparatus for electrochemical oxidation in front of the spectrometer

Here A denotes the storage flask where samples can be degassed before they are measured. To avoid any loss of solvent the nitrogen stream was saturated with the very same solvent before it enters the sample solution. In order to transport the sample through the whole system nitrogen pressure has been applied after degassing. To avoid contamination with oxygen only gas tight Teflon tubes were utilized to transport the sample solution. The space inside the magnet B is displayed from the backside in figure 15 in a larger view. The valve C is used to regulate the flow rate. It has been installed at the end of the apparatus where the uptake of oxygen does not matter anymore. To measure the flow rate, the waste D has been replaced by a graduated cylinder, and the time in-between two 1 ml marks was measured. E is the potentiostat and F a common voltmeter to measure the current that flows during the measurement, which provides information on the potential in the cell if the flow rate is known. G is peristaltic pump which was used to pump an electrolyte solution in the compartment of the CE. During a measurement it is disconnected, and this compartment was closed by short circuiting the tubes from in and outlet.

A quartz capillary was fixed in an ER 4102 ST-O cavity from Bruker, which is the instruments standard resonator, and connected with the reaction cell, shown in figure 15.

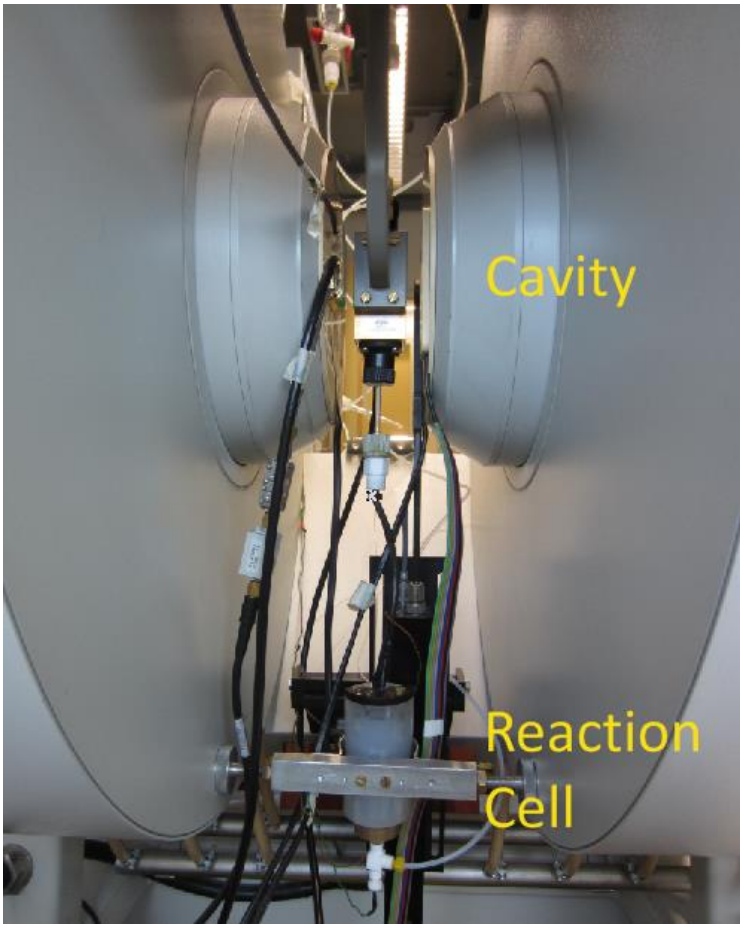

Figure 14: Electrochemical reaction cell inside the magnet

The reaction cell, which is displayed in figure 15, contains a cylindrical porous Teflon membrane, to separate the half-cells. Working and counter electrode consist of carbon and are placed inside (WE) and outside (CE) of the membrane, were they are contacted via a tungsten wire. The wire contacting the WE is mounted in the inlet for the sample solution at the bottom of the cell. It is covered by a Teflon tube, in order to ensure that oxidation or reduction only occurs in the centre of the cell.

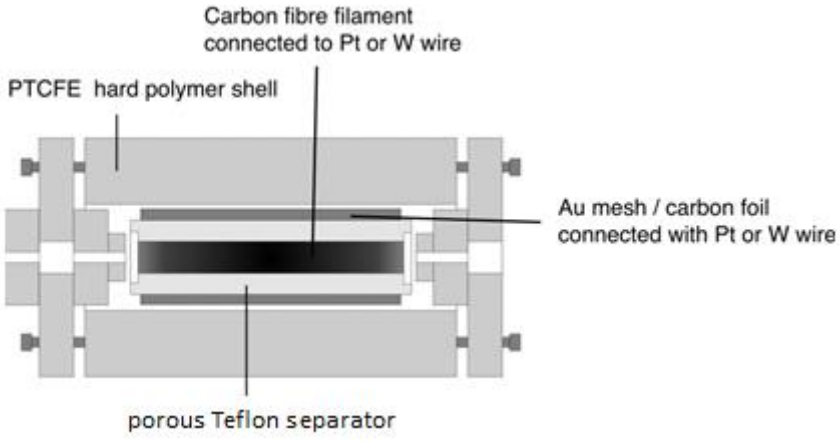

Figure 15: Cross section of the electrochemical reaction cell

ENDOR measurements were performed with a special EN 801 cavity from Bruker. In the utilized system the radiofrequency is generated outside of the resonator, which is advantageous in respect to temperature, since the rf-generator produces heat.

An AVANCE DPX200 spectrometer from Bruker, which is a 200 MHz instrument, was used for NMR measurements.

4.4 Sample Preparation

Chemical oxidations were performed under nitrogen atmosphere in the degassed solvents. The oxidizing agent was used as limiting reactant in a concentration of approximately 0.5 mM. The violet colour of dissolved ZnTPP changes to dark and/or green after a couple of minutes, dependent on the oxidizing agent. Due to the fact that the process of dissolving ZnTPP and the chemical oxidation is relatively slow in the used solvents the solutions were put in an ultrasonic bath for 10 min. Approximately three droplets of these solutions were transferred in a glass capillary and further degassed by three freeze-pump-thaw cycles. Liquid nitrogen was used to freeze the samples, which were finally sealed under vacuum with a gas flame. The sealed samples were directly measured after defrosting.

Electrochemical oxidations were performed in the flow system, described in chapter 4.3. The concentration of the supporting electrolyte was chosen to be 20 mM, the one of the ZnTPP 0.5 mM. At least 20 ml of a sample was prepared. Before measuring the samples were degassed in the storage flask for 10 min by bubbling nitrogen through the solution. The electrical potential and the flow rate were optimized to get the most intense signal.

4.5 Results from the NMR Measurements

A cut-out of the NMR spectrum of the synthesised ZnTPP in $DCCl_3$ after being chromatographically purified is displayed in figure 16.

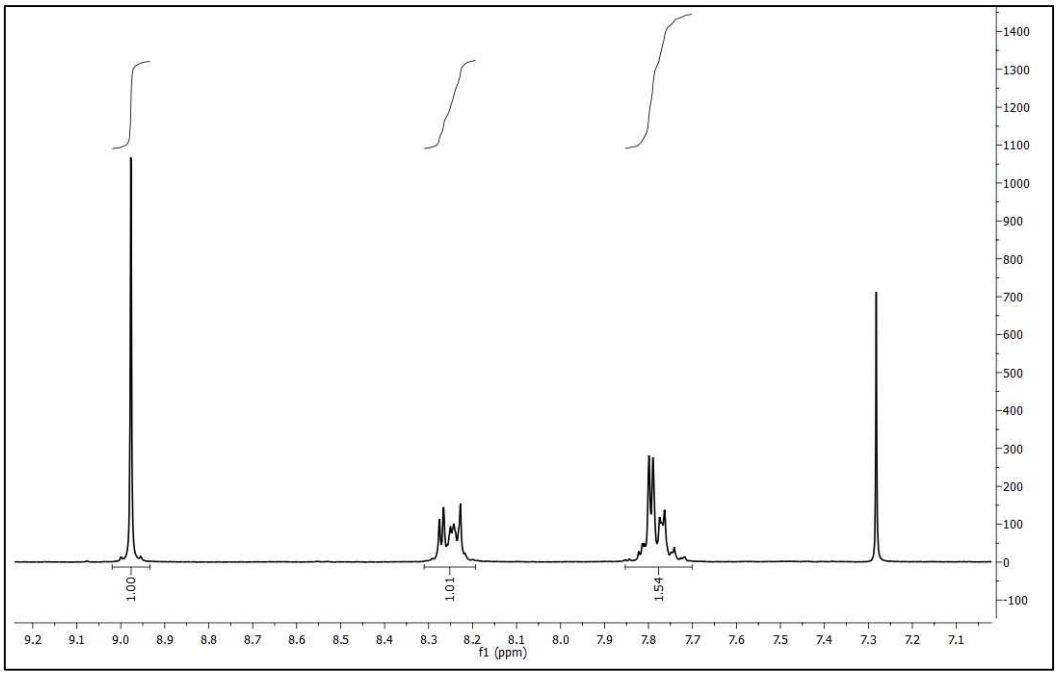

Figure 16: NMR spectrum of ZnTPP in $DCCl_3$

The signal at 7.3 ppm corresponds to non-deuterated chloroform. The aromatic protons of the phenyl rings give two multiplets, due to the fact that dissolved ZnTPP is not perfectly planar in D_{4h} symmetry. The highly shifted singlet at approximately 9 ppm corresponds to the vinylic protons of the porphyrin system and displays distinct ^{13}C-satelites. This rather high chemical shift was also observed for PdTPP, thus it is assumed that the electron withdrawing effect of the metal centre is relatively strong. Therefore these protons can be considered relatively reactive. The comparison of the integral gives a perfect 2:5 ratio between the vinylic and the aromatic protons, which was expected.

4.6 Results from the ENDOR Measurements

The ENDOR system is not easily combined with the electrochemical flow apparatus. On one hand this is related to the long measuring times, which would require large amounts of sample solution, on the other the investigated system is not easily saturated by radiation. This problem is increased if one moves the sample. Therefore chemically oxidized systems had to be taken. The measurements were performed on four systems, which were 1 mM solutions of ZnTPP oxidized by Magic Blue in MeCN, oDCB, Toluene and Hexafluoro-2-propanol. The maximum available microwave and radio frequency power was not sufficient to saturate the corresponding transitions in these systems. In every system two broad lines centred at 14.5 MHz were observed, when pumping at the central line. However, only the spectra in MeCN and DCB, which are displayed in figures 17 and 18 contained useful information.

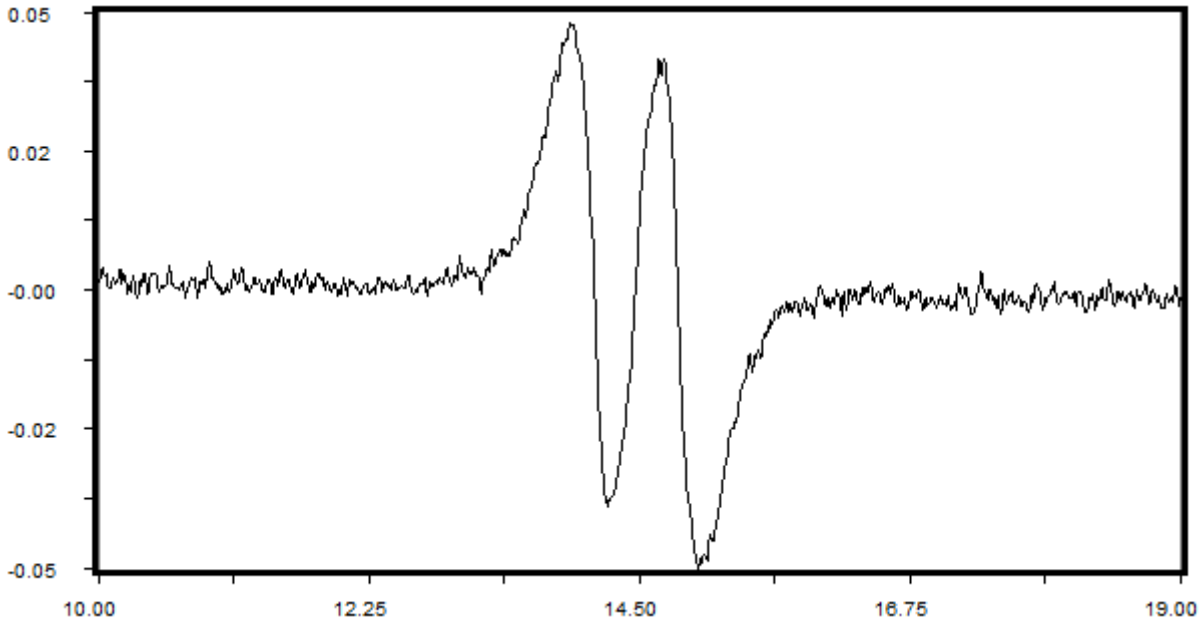

Figure 17: ENDOR spectrum of 0.5 mM ZnTPP radical cation, oxidized by MB, in MeCN plotted in arbitrary units of intensity versus MHz

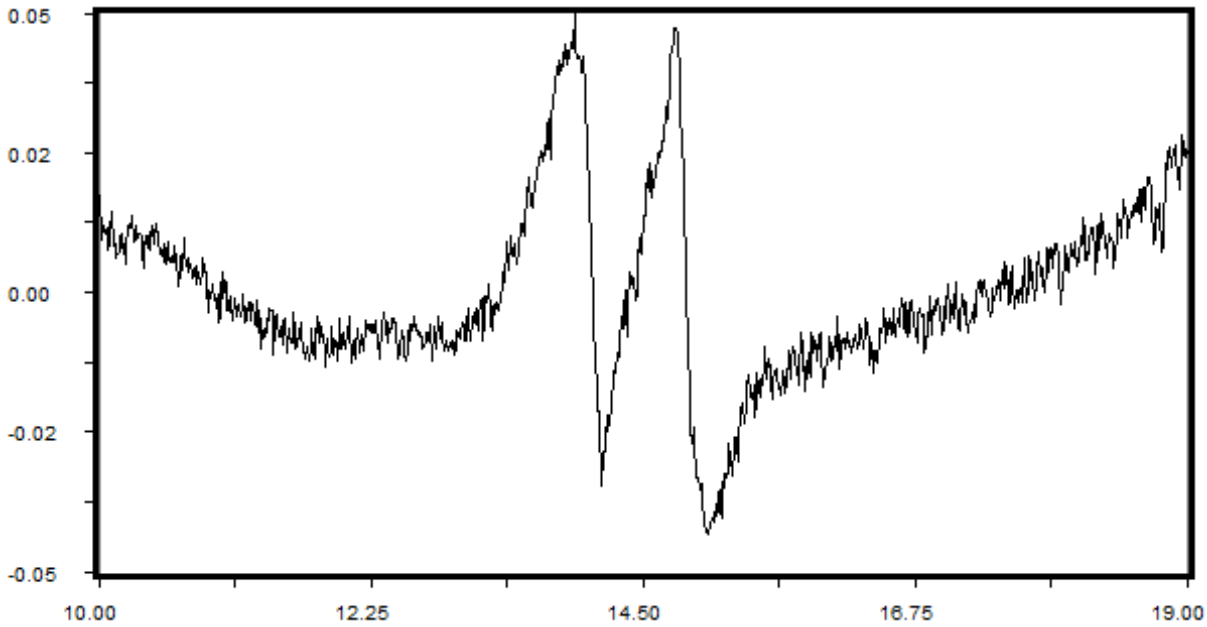

Figure 18: ENDOR spectrum of 0.5 mM ZnTPP radical cation, oxidized by MB, in DCB plotted in arbitrary units of intensity versus MHz

Zooming in on both spectra indicated that there are actually more lines, three doublets would be expected, but due to the poor resolution only the one splitting constant was obtained from the ENDOR spectra. The obtained values in G in MeCN are compared with literature in table 3, where the difference from MeCN to PrCN, which was used in literature [37], was considered negligible. The experimental 4N-splitting was measured from CW-spectra at low temperature in winsim2002. The 4H-splitting, which is marked bold in table 3, is taken from the ENDOR spectrum, the other two obtained by simulating in winsim2002, where the best fit was taken as indicator.

hfc	Experimental	Fukuzumi [2]	Borg [37]
4N	1.5 - 1.6	2.04	1.58
4Ha	**0.248**	0.32	
8Hb	0.323	0.36	0.316
8Hc	0.379	0.46	

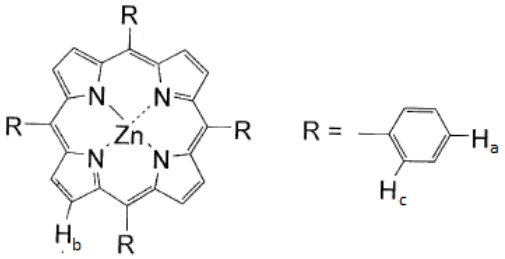

Table 2: Comparison of hyperfine splitting constants and a proposed assignment to specific nuclei

The assignment of hyperfine splitting constants to specific nuclei was estimated from simulations, where best fit was assumed to correspond to the right configuration.

4.7 Results for Chemically Oxidized Systems

A change of colour was observed for a few systems, but no ESR signal could be detected. This circumstance was observed for the following combinations of oxidizing agent and solvent $AgClO_4$/MeCN, DBPO/MeCN, (Bis(trifluoracetoxy)iod)benzene/Hexafluoro-2-propanol and $(NH_4)_2Ce(NO_3)_6$/PrCN. It is important to point out, that just a quick pre-screening was performed to identify the most promising systems, thus no definitive conclusions should be drawn from the information on these systems.

Due to the relatively small molecular weight of $NOClO_4$ sample preparation required an additional pipet step, which is not desirable. This oxidizing agent was tested in oDCB and DCM. However, the signal intensity was relatively small, which indicates that the reaction is not happening quantitatively in this solvent. A spectrum is displayed in figure 20 in Appendix B.

The oxidizing agents that performed best in a variety of solvents are Magic Blue and the Ru(III)-complex used by Fukuzumi, which lead to almost identical spectra in MeCN, DCB, DCM and CF. The temperature dependence and long term stability of these systems was investigated. To test long term stability samples were taken from the reaction mixture at different times and already sealed capillaries were measured at different times as well. This indicated that the formation of the radical takes a few minutes, dependent on the solvent, however no further kinetic studies have been performed on the oxidation process itself.

For thermal stability the dependence of the double Integral on temperature was investigated. As long as the signal loss is only related to thermal motion (see chapter 2.4 equations (2.18) and (2.19)) it should be approximately linear. If something else happens, like dimerization or thermal degradation, a significant deviation is observed. For determining equilibrium constants of dimerization processes e.g. this effect has been utilized in literature. [38] The

temperature dependence of the signal intensity in the solvents MeCN, oDCB and CF is displayed in diagram 1, were only data from spectra with one equivalent of ZnTPP in respect to the oxidizing agent was used. The spectra were recorded in steps of 10K in the following temperature ranges: for MeCN 233-333K, oDCB 258-388K, and for CF 220-320K. The ranges were determined by freezing and boiling point of the solvents.

It is important to point out that the signal loss after the break points in diagram 1 is irreversible for every system investigated. Comparative measurements of samples at room temperature before and after heating slightly above this point showed further, that this signal loss is in a magnitude of 20-30%. Data for DCM is not displayed due to the fact that after a short time an unidentified green solid precipitated in the sealed sample capillary. The ESR signal disappeared simultaneously.

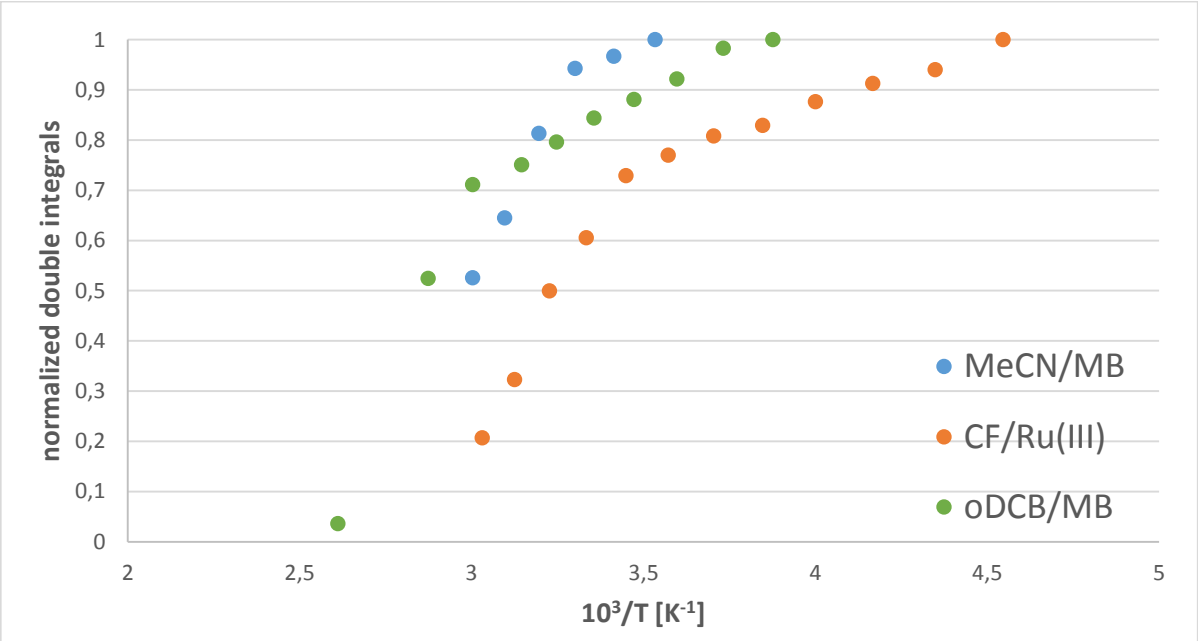

Diagram 1: Curie plots for chemically oxidized systems

Even though the temperature dependent measurements were performed with different amounts of excess ZnTPP, no kinetic information could be obtained from these spectra, due to the appearance of an additional unidentified signal. A representative collection of the corresponding spectra is displayed in Appendix B. Due to this additional signal ten lines are observed in the first derivative representation, as opposed to the nine expected from theory. The corresponding absorption spectra consist of two bands as well. This additional signal was observed in all systems, independent of the solvent or the oxidizing agent. Further NMR and electrochemical studies confirmed, that it is not related to impurities in the synthesized ZnTPP.

Moreover spectra of all the paramagnetic oxidizing agents have been recorded to see if they overlap with the signal of ZnTPP radical cation, which would be expected if the chemical conversion is not quantitative.

Several attempts to simulate the spectra in order to get good values for the line width in winsim2002 and ESR-ET have been executed in order to be able to estimate kinetic information at least. The hyperfine structure, which consists of 3645 line (predicted by equation (2.24)) if one neglects the aromatic protons in ortho-position, is too complex for ESR-ET. In winsim2002 simulations with fixed hyperfine splitting constants and an assumed perfect Lorentzian line shape showed trends, but no absolute values, due to the increased signal to noise ratio at higher temperatures. The only trend, which is assumed to be useful, is displayed in diagram 2. Here the line width is plotted temperature over viscosity dependent for the system oDCB/MB, where one equivalent of ZnTPP was used with respect to the oxidizing agent.

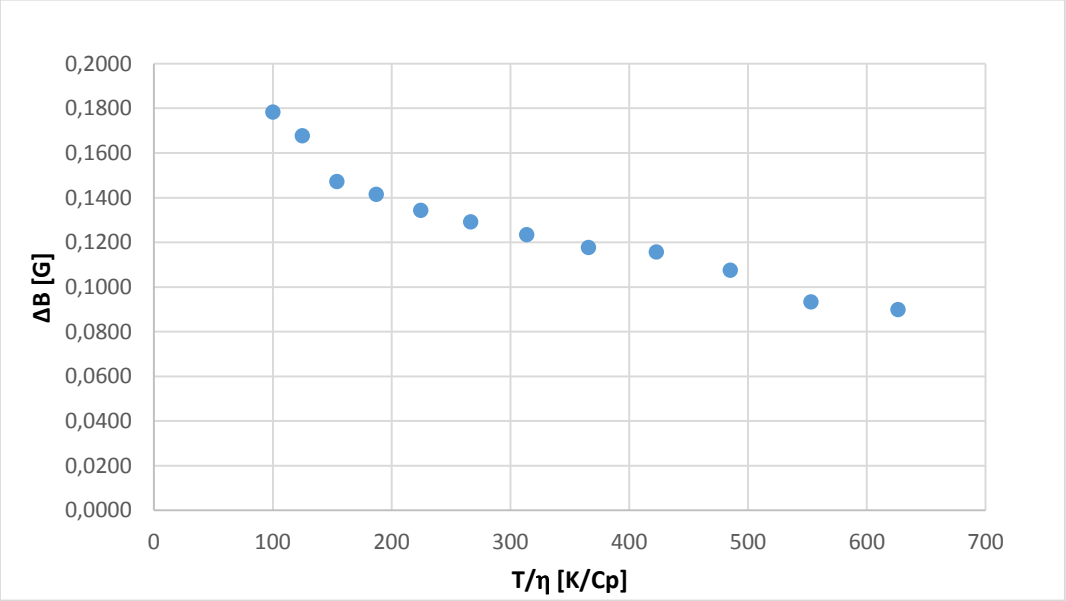

Diagram 2: Linebroadening in oDCB dependent on temperature

This function resembles literature [32] where this behaviour was shown for conditions outside of the usual linear region, where line broadening experiments are usually executed.

4.8 Results for Electrochemically Oxidized Systems

Before measuring ZnTPP the electrochemical cell was tested with a 1mM solution of 1,4-dicyanobenzene (Aldrich 98%) in MeCN, which is known from literature. [39]

Considering the solubility of the supporting electrolyte experiments were performed in MeCN and PrCN. Due to the already mentioned issues with solubility, which is obviously not improved by the supporting electrolyte, no useful spectra could be recorded in MeCN. The most intense signal in PrCN was obtained at a flow rate of 1.5 ml/min and a current of 8.64 mA with a modulation amplitude of 500 mG. It can be simulated nicely with the obtained hyperfine splitting constants in winsim2002, see figure 19. The deviation is mainly related to the over modulation, which was used to get a sufficiently intense signal, and the confinement of the simulation to a Lorentzian line shape, which was done to reduce the number of variables. However, no additional signal from side products is observed, as it is the case for chemically oxidized systems. Further the method is highly reproducible, thus it can be used for further kinetic investigations on metal porphyrins, which was the aim of this thesis.

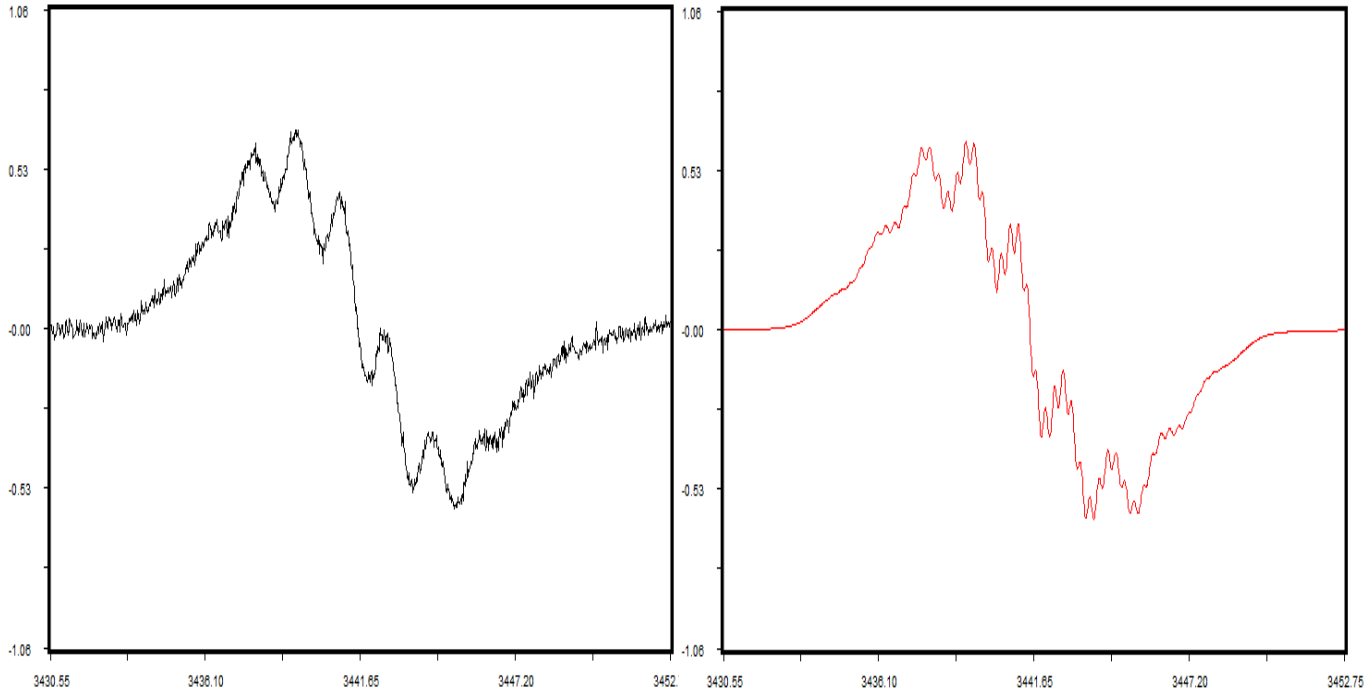

Figure 19: ESR spectrum of electrochemically generated ZnTPP radical cation in PrCN plotted in arbitrary units of intensity versus G (left) and the simulation in winsim2002 (right)

Moreover the green color of the ZnTPP radical cation could be confirmed with these experiments and the relatively fast decay of the radical became visible. A short time after the green solution of the radical leaves the cavity it turns dark violet in the tubes. In the waste, after coming in contact with oxygen, the solution displayed a deep red color.

4.9 Discussion

In the present work several ways to generate the radical cation of ZnTPP have been tested. However, chemical oxidation with metal ions, organic molecules and organic radicals always yielded additional products, of which at least one is paramagnetic. Due to the fact that this additional signal hasn´t been observed in the electrochemical system, it is assumed, that it results from reactions with the oxidizing agents. The NMR data indicates highly activated vinylic protons, which are very likely to undergo electrophilic substitution reactions, which was shown in literature before for the oxidation with molecular bromine. [1]

Further, the unknown kinetics of the chemical oxidations and the decay of the radical, which was observed in the electrochemical flow apparatus, complicate the interpretation of the spectra from these systems.

Moreover, the impact of heating in the ultrasonic bath and during the sealing of the samples is not known yet. Considering the information from the temperature dependent measurements, which show, that the radical transforms irreversibly at slightly elevated temperatures, suggest that this impact is not negligible.

In conclusion there are too many variables in the methodical approach of chemical oxidations, to obtain useful results.

Even though the electrochemical oxidations work quite well, the problem of dissolving the analyte still remains. Usually line broadening experiments are set up in a concentration range which covers at least two orders of magnitude to obtain statistically significant results. Unfortunately the investigated system is highly limited in respect to the concentration range which can be exploited, which has been found for all systems to be somewhere between 0.4-4 mM. Additionally the supporting electrolyte must be soluble in the solvent as well, therefore the amount of useful solvents for further research is limited.

Another limitation for further research is in respect to the temperature range. The radical is stable in the lower temperature range, where line broadening from dipolar interactions and maybe even tunnelling is influencing the spectra and the electron self-exchange. The problem with dipolar interactions is discussed theoretical in a rather recent publication by K. M. Shalikov [40] and still content of current research. Further tunnelling can become the

dominant mechanism of ET at low temperatures, which lowers the observed activation barrier.

4.10 Conclusion

The rate constants published by Fukuzumi remain questionable, due to the fact that they cannot be reproduced. The irreproducibility is related to the unexpected chemical reactivity and stability of his system. Moreover theoretical approximations, which are not considered to be valid any more, were used to calculate them from values that were simulated with hyperfine splitting constants, which do not correspond to older literature and our experiments. In the present work a reproducible method for further investigation of electron self-exchange kinetics of ZnTPP has been introduced. This electrochemical method will be used to determine rate constants dependent on solvent properties, to determine the type of ET reaction, and on the temperature, to calculate activation barriers. Further the products, which are formed after oxidation, will be identified by HPLC-MS.

List of References

[1] P. C. Dave, D. Srinivas; Eur. J. Inorg. Chem. 447 (2002)

[2] S. Fukuzumi et al; J. Porphyrins Phtalocyanines; 7; 328 (2003)

[3] S. Fukuzumi et al; J. Am. Chem. Soc.; 124; 10974 (2002)

[4] J.P. Roth et al; J. Am. Chem. Soc.; 9; 125 (2003)

[5] R. A. Marcus; Pure & Appl. Chem.; 69; 13 (1997)

[6] N. Sutin; Progr. Inorg. Chem.; 30; 441 (1983)

[7] J.A. Weil, J.R. Bolton; *EPR: Theory and Practical Applications*; 2nd Edition; Wiley; 2007

[8] F. Gerson, W. Huber; *ESR Spectroscopy of Organic Radicals*; Wiley-VCH, 2003

[9] H. Kurreck, B. Kirste, W. Lubitz; *ENDOR Spectroscopy of Radicals in Solution*; VCH; 1988

[10] R.A. Marcus; J. Chem. Phys; 24; 966 (1956)

[11] R.A. Marcus; J. Chem. Phys; 26; 867 (1957)

[12] R.A. Marcus; J. Chem. Phys; 26; 872 (1957)

[13] W.F. Libby; J. Phys. Chem.; 56; 863 (1952)

[14] D. R. Rosseinsky; Comments on Inorganic Chemistry; 3; 153 (1984)

[15] R.M. Fuoss; J. Am. Chem. Soc.; 80; 5059 (1958)

[16] M. Eigen; Zeitschrift für physikalische Chemie (München); 1; 176 (1954)

[17] P. W. Atkins; *Physikalische Chemie*; 3rd Edition; VCH; (1987)

[18] S.F. Nelsen et al; J. Am. Chem. Soc.; 109; 677 (1987)

[19] T. Holstein; Philosophical Magazine B; 37; 49 (1978)

[20] M. J. Weaver, E. L. Yee; Inorganic Chemistry; 19; 1936 (1980)

[21] R. A. Marcus, N. Sutin; Biochimica et Biophysica Acta; 811; 265 (1985)

[22] G. Grampp et al; J Chem. Soc., Perkin Transactions 2; 178 (2002)

[23] J.R. Miller; J. Am. Chem. Soc.; 106; 3047 (1984)

[24] N. Sutin; Acc. Chem. Res.; 15; 275 (1982)

[25] M.J. Weaver; Chem. Rev.; 92; 463 (1992)

[26] H.A. Kramers; Physica (The Hague); 7; 284 (1940)

[27] P. Zeeman; Verhandlungen der Physikalischen Gesellschaft zu Berlin; Nr. 7; 128 (1896)

[28] O. Stern, W. Gerlach; Zeitschrift für Physik; 9; 349 (1922)

[29] G. E. Uhlenbeck, S. Goudsmit, Naturwissenschaften, 13, 953 (1925)

[30] K. Zavoisky; J. Phys. USSR; 9; 211 (1945)

[31] G. Feher, Phys. Rev., 103, 834 (1956)

[32] B. Berner, D. Kievelson; J. Phys. Chem; 83; 1406 (1979)

[33] G. Grampp; Spectrochimia Acta Part A; 54; 2349 (1998)

[34] G. Jeschke; *Einführung in die ESR-Spektroskopie*; VO-Skript Uni Konstanz (1998)

[35] G. Wagner; *Anorganisches präparatives Praktikum*; Franz Deuticke (1947)

[36] A. D. Adler et al; J. Inorg. Nucl. Chem.; 32; 2443 (1970)

[37] C. Borg et al; J. Am. Chem. Soc.; 92; 3451 (1970)

[38] G. Grampp et al; Spectrochimia Acta Part A; 58; 1219 (2002)

[39] B. Mladenova et al; Z. Phys. Chem; 220 543 (2006)

[40] K. M. Shalikov; Appl. Magn. Reson.; 38; 237 (2010)

Appendix A: Detailed Kinetics of ET

The assumptions from chapter 1.9 for an ET process according to equation (1.17) are summarized in equations I-III. Starting from this a step by step instruction on how to obtain equation (1.21) is shown.

$$I\text{: } k_{obs}[A][D] = k_{diff}[S]$$

$$II\text{: } \frac{\partial[P]}{\partial t} = 0 = k_d[A][D] + k_{-ex}[S] - (k_{ex} + k_{-d})[P]$$

$$\rightarrow [S] = \frac{(k_{ex} + k_{-d})[P] - k_d[A][D]}{k_{-ex}}$$

$$III\text{: } \frac{\partial[S]}{\partial t} = 0 = k_{ex}[P] - \left(k_{-ex} + k_{diff}\right)[S]$$

$$\rightarrow [P] = \frac{\left(k_{-ex} + k_{diff}\right)[S]}{k_{ex}}$$

Inserting equation III in equation II leads to a common expression of [S] in equation IV.

$$[S] = \frac{\left(k_{-ex} + k_{diff}\right)[S]}{k_{ex}} * \frac{(k_{ex} + k_{-d})}{k_{-ex}} - \frac{k_d[A][D]}{k_{-ex}}$$

$$[S] - \frac{\left(k_{-ex} + k_{diff}\right)[S]}{k_{ex}} * \frac{(k_{ex} + k_{-d})}{k_{-ex}} = -\frac{k_d[A][D]}{k_{-ex}}$$

$$[S] * \left[1 - \frac{\left(k_{-ex} + k_{diff}\right)}{k_{ex}} * \frac{(k_{ex} + k_{-d})}{k_{-ex}}\right] = -\frac{k_d[A][D]}{k_{-ex}}$$

$$[S] * \left[\frac{(k_{ex} * k_{-ex}) - \left(k_{-ex} + k_{diff}\right) * (k_{ex} + k_{-d})}{k_{ex} * \boldsymbol{k_{-ex}}}\right] = -\frac{k_d[A][D]}{\boldsymbol{k_{-ex}}}$$

$$[S] = -\frac{k_d[A][D] * k_{ex}}{(k_{ex} * k_{-ex}) - \left(k_{-ex} + k_{diff}\right) * (k_{ex} + k_{-d})}$$

$$[S] = -\frac{k_d[A][D] * k_{ex}}{(\boldsymbol{k_{ex}} * \boldsymbol{k_{-ex}}) - (\boldsymbol{k_{ex}} * \boldsymbol{k_{-ex}}) - (k_{-ex} * k_{-d}) - \left(k_{ex} * k_{diff}\right) - \left(k_{-d} * k_{diff}\right)}$$

$$IV\text{: } [S] = \frac{k_d[A][D] * k_{ex}}{(k_{-ex} * k_{-d}) + \left(k_{ex} * k_{diff}\right) + \left(k_{-d} * k_{diff}\right)}$$

Inserting equation IV in equation I yield the deserved expression of k_{obs}.

$$k_{obs}[\boldsymbol{A}][\boldsymbol{D}] = k_{diff} * \frac{k_d[\boldsymbol{A}][\boldsymbol{D}] * \ k_{ex}}{(k_{-ex} * k_{-d}) + (k_{ex} * k_{diff}) + (k_{-d} * k_{diff})}$$

$$k_{obs} = \frac{k_{diff} * \ k_d * \ k_{ex}}{(k_{-ex} * k_{-d}) + (k_{ex} * k_{diff}) + (k_{-d} * k_{diff})}$$

$$k_{obs} = k_d * \left[\frac{(k_{-ex} * k_{-d}) + (k_{ex} * k_{diff}) + (k_{-d} * k_{diff})}{k_{diff} * \ k_{ex}}\right]^{-1}$$

$$k_{obs} = k_d * \left[\frac{k_{-ex} * k_{-d}}{k_{diff} * \ k_{ex}} + \frac{k_{ex} * k_{diff}}{k_{diff} * \ k_{ex}} + \frac{k_{-d} * k_{diff}}{k_{diff} * \ k_{ex}}\right]^{-1}$$

$$k_{obs} = k_d * \left[1 + \frac{k_{-d}}{k_{ex}} * \left(1 + \frac{k_{-ex}}{k_{diff}}\right)\right]^{-1}$$

Appendix B: Measured Spectra

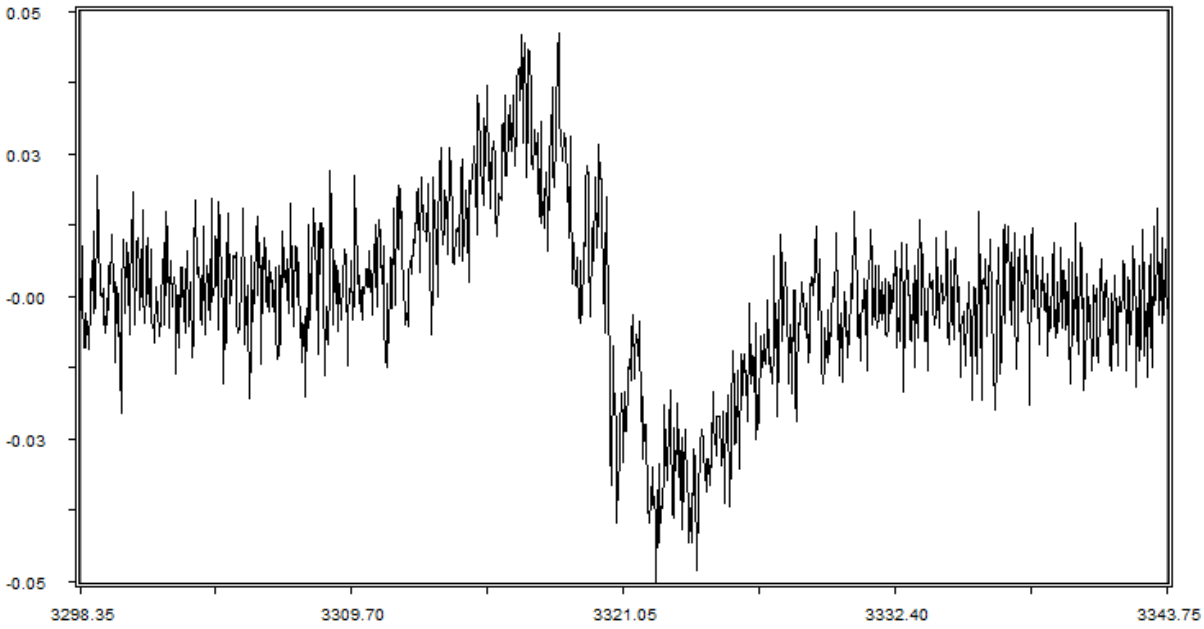

Figure 20: Spectrum of 0.5 mM ZnTPP radical cation oxidized by $NOClO_4$ in oDCB at RT

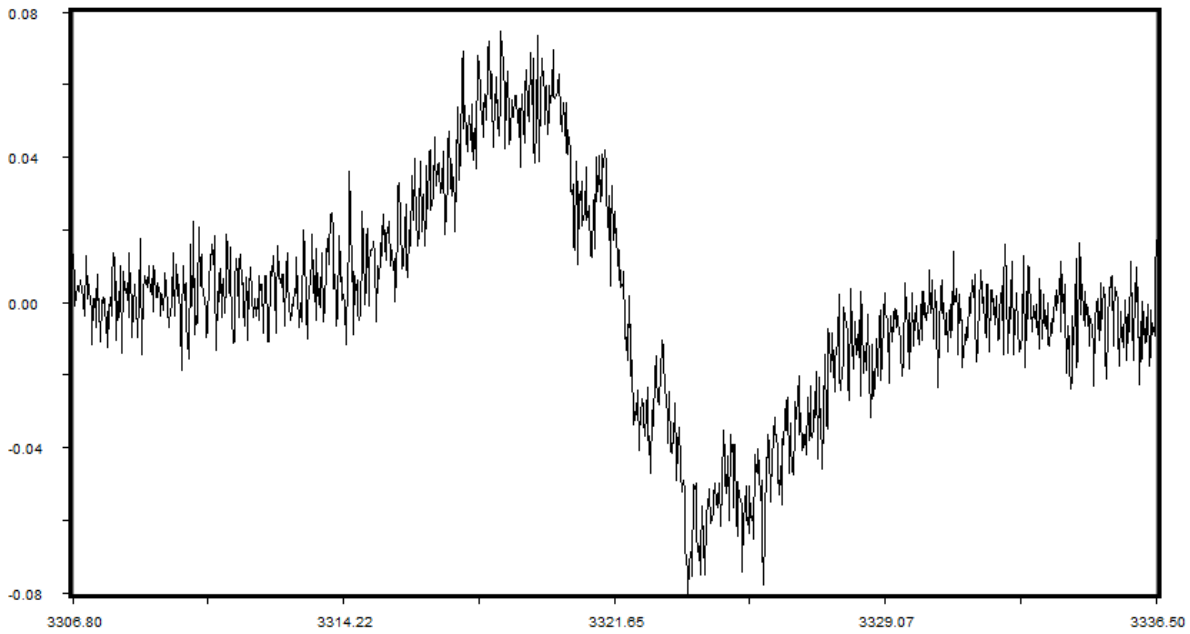

Figure 21: Spectrum of 0.5 mM ZnTPP radical cation oxidized by Ru(III) in DCM at RT

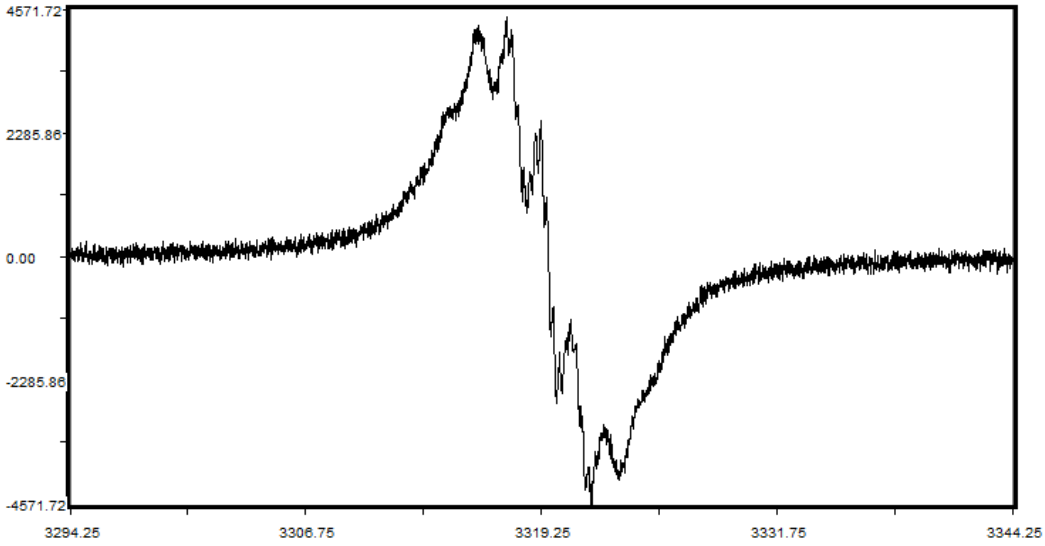

Figure 22: Spectrum of 0.5 mM ZnTPP radical cation oxidized by MB in oDCB at 258K

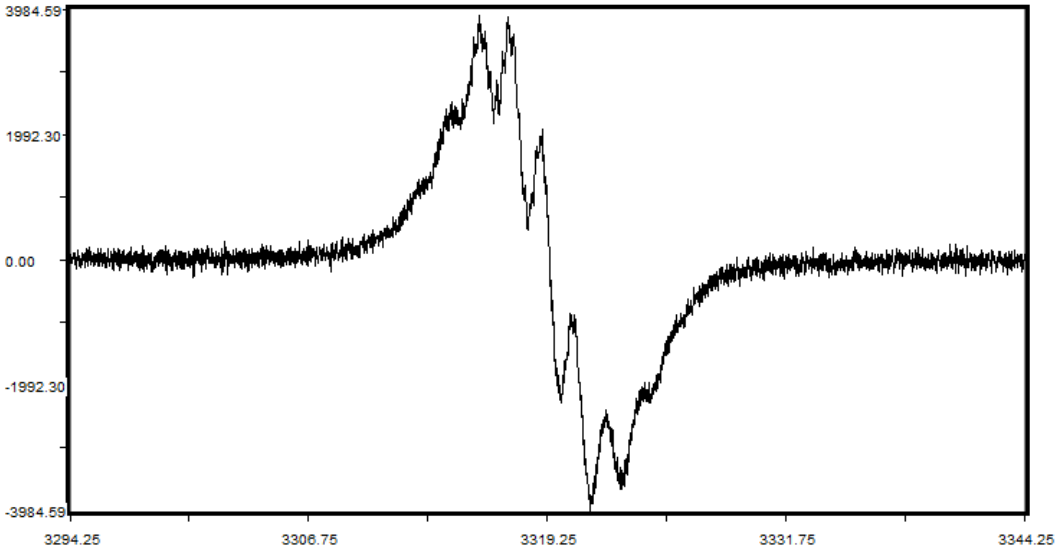

Figure 23: Spectrum of 0.5 mM ZnTPP radical cation oxidized by MB in oDCB at 298K

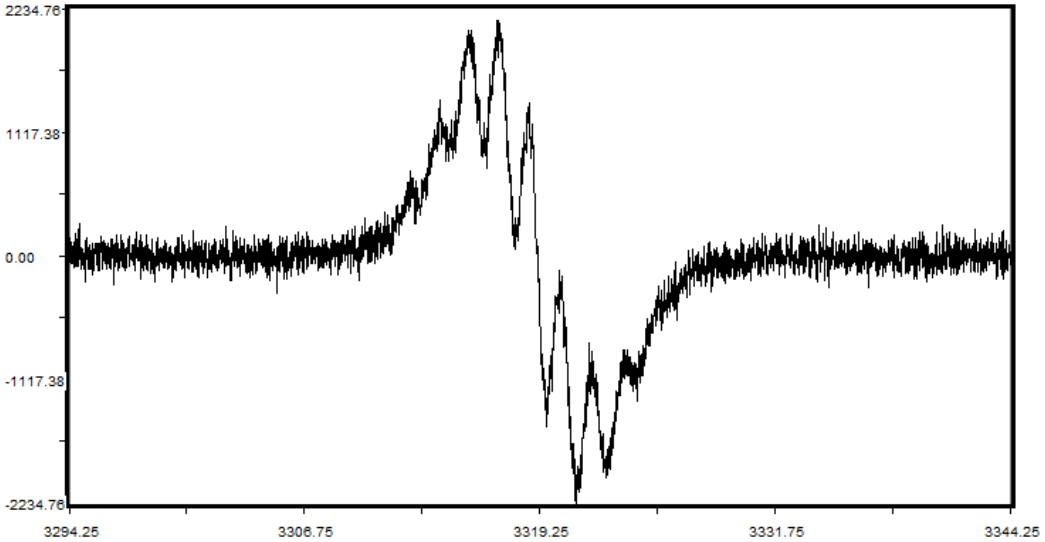

Figure 24: Spectrum of 0.5 mM ZnTPP radical cation oxidized by MB in oDCB at 338K

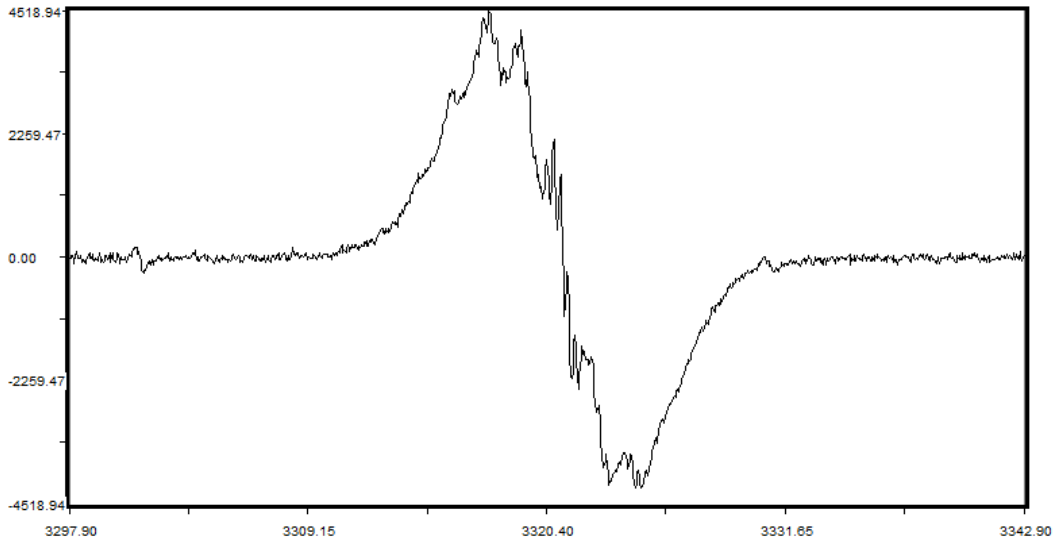

Figure 25: Spectrum of 0.5 mM ZnTPP radical cation oxidized by Ru(III) in CF at 220K

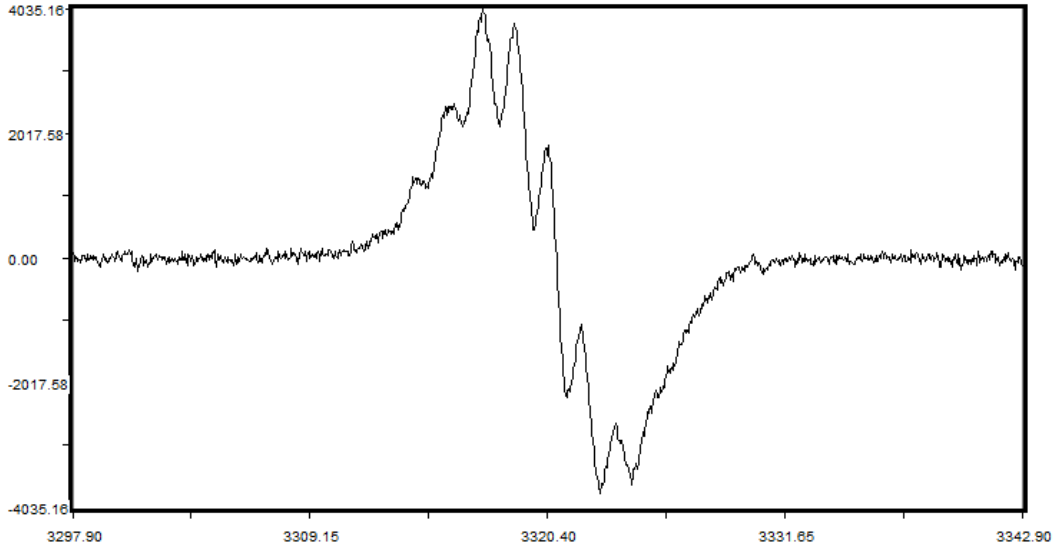

Figure 26: Spectrum of 0.5 mM ZnTPP radical cation oxidized by Ru(III) in CF at 290K

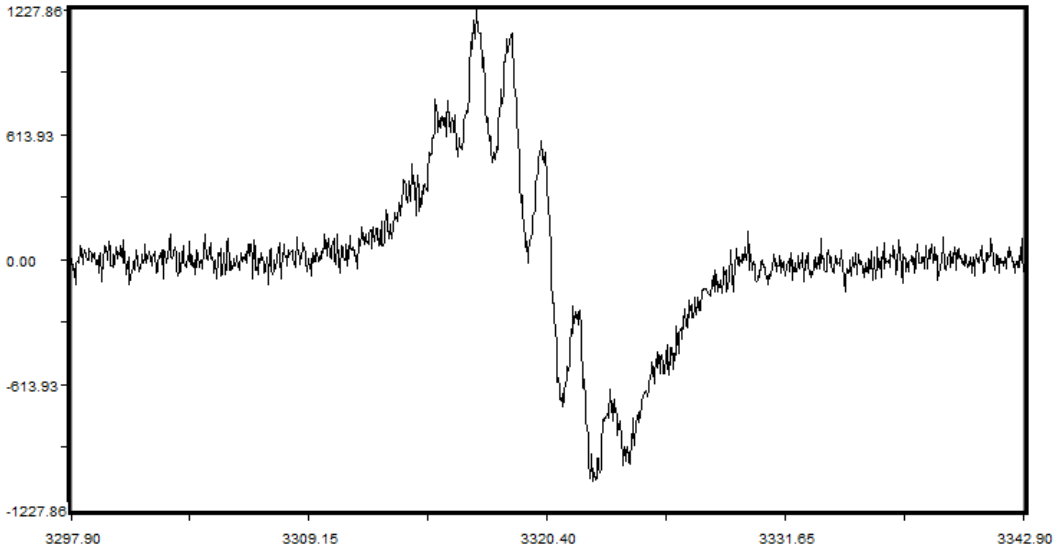

Figure 27: Spectrum of 0.5 mM ZnTPP radical cation oxidized by Ru(III) in CF at 330K

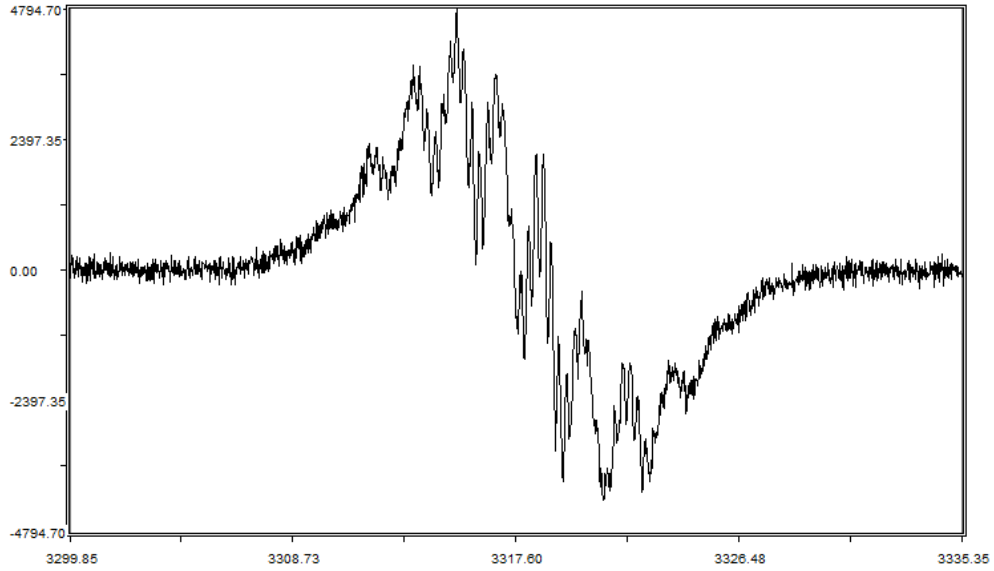

Figure 28: Spectrum of 0.5 mM ZnTPP radical cation oxidized by MB in MeCN at 233K

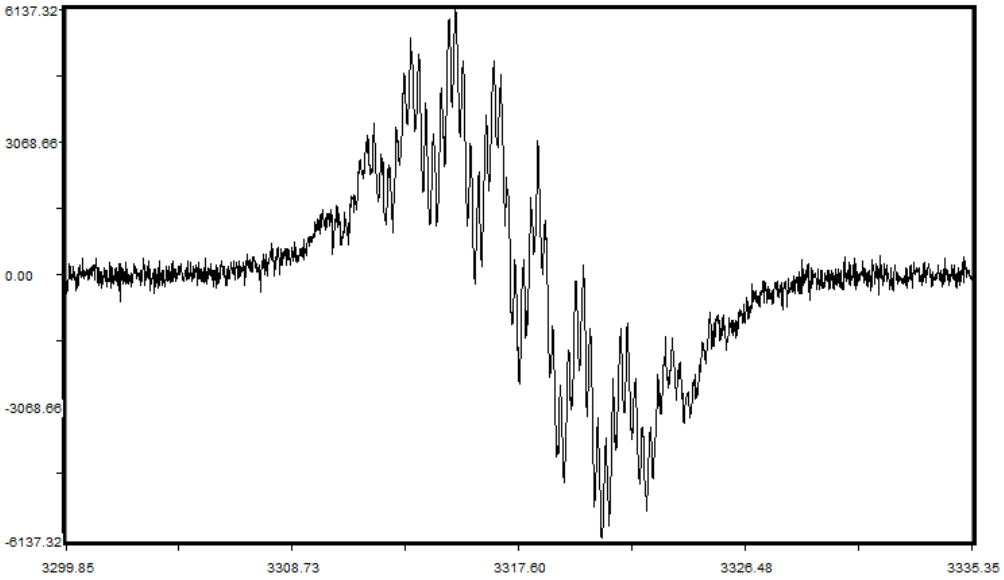

Figure 29: Spectrum of 0.5 mM ZnTPP radical cation oxidized by MB in MeCN at 293K

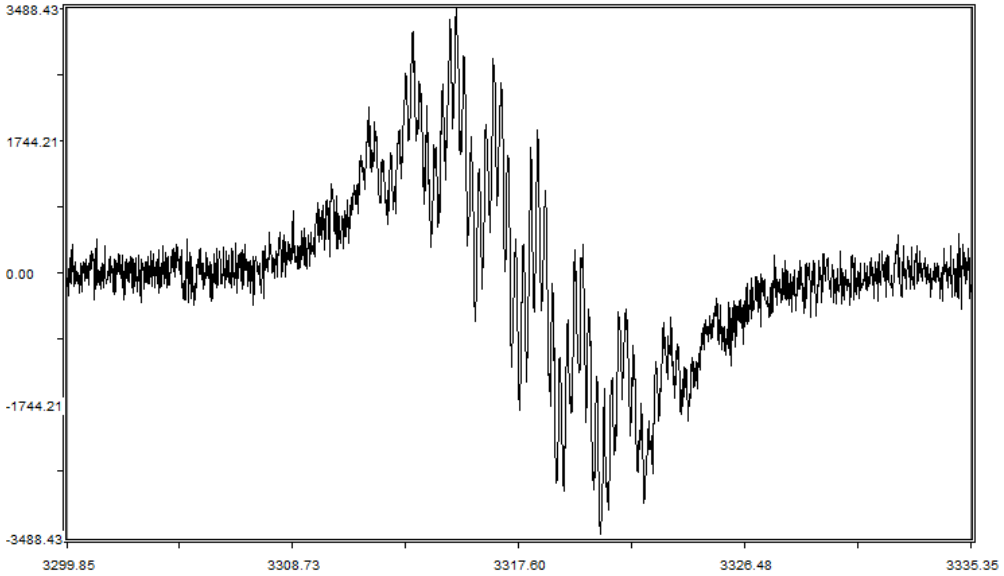

Figure 30: Spectrum of 0.5 mM ZnTPP radical cation oxidized by MB in MeCN at 333K